1998-06

Structure and variability of the mesoscale circulation in the Caribbean Sea as deduced from satellite altimetry

Pibernat, Luis

Monterey, California. Naval Postgraduate School

NAVAL POSTGRADUATE SCHOOL
Monterey, California

THESIS

STRUCTURE AND VARIABILITY OF THE MESOSCALE CIRCULATION IN THE CARIBBEAN SEA AS DEDUCED FROM SATELLITE ALTIMETRY

by

Luis Pibernat

June, 1998

Thesis Advisor: Pierre-Marie Poulain
Second Reader: Newell Garfield

Approved for public release; distribution is unlimited

REPORT DOCUMENTATION PAGE

Form Approved
OMB No. 0704-0188

1. AGENCY USE ONLY *(Leave blank)*	2. REPORT DATE	3. REPORT TYPE AND DATES COVERED
	June, 1998	Master's Thesis

4. TITLE AND SUBTITLE
STRUCTURE AND VARIABILITY OF THE MESOSCALE CIRCULATION IN THE CARIBBEAN SEA AS DEDUCED FROM SATELLITE ALTIMETRY

5. FUNDING NUMBERS

6. AUTHOR(S)
Luis Pibernat

7. PERFORMING ORGANIZATION NAME(S) AND ADDRESS(ES)
Naval Postgraduate School
Monterey, CA 93943-5000

8. PERFORMING ORGANIZATION REPORT NUMBER

9. SPONSORING / MONITORING AGENCY NAME(S) AND ADDRESS(ES)

10. SPONSORING / MONITORING AGENCY REPORT NUMBER

11. SUPPLEMENTARY NOTES
The views expressed in this thesis are those of the author and do not reflect the official policy or position of the Department of Defense or the U.S. Government.

12a. DISTRIBUTION / AVAILABILITY STATEMENT
Approved for public release; distribution is unlimited.

12b. DISTRIBUTION CODE

13. ABSTRACT ***(maximum 200 words)*** Four years of Topex/Poseidon (T/P) and European Remote Sensing Satellite (ERS) altimetry data in the Caribbean Sea are used to describe the structure and variability of the mesoscale circulation in this area. These results are compared with satellite-derived sea surface temperature (SST) and drifter trajectories for the same period of time. Contour maps of sea surface height anomalies made for each 10-day period (T/P data) reveal the formation and evolution of anticyclonic and cyclonic mesoscale features in the central part of the Caribbean Sea during the entire period studied. These features move westward at average speeds between 10 and 15 cm/s, growing in amplitude up to 25 cm. Also, a quasi-permanent gyre is detected in the Golfo de los Mosquitos (coast of Panama and Colombia). The sense of rotation of this gyre is shown to be modulated seasonally. Enhanced relative clockwise and counterclockwise rotation are observed during the rainy season (June-October) and the dry/windy season (January-April), respectively. No strong mesoscale anomalies are detected in the eastern part of the Caribbean Sea where they are expected. A seasonal cycle is found in the sea level anomaly (SLA) derived from T/P and ERS-1 data due to steric effects. Upwelling is observed near the coast of Venezuela during the dry season. A comparison of SLA with SST is made and good correlation is observed at some locations. Drifter trajectories contemporaneous with SLA data agree well with the sense of rotation of strong features, but the drifter speeds are twice the absolute geostrophic currents calculated from SLA.

14. SUBJECT TERMS
Caribbean Sea, Topex/Poseidon (T/P), ERS-1, Mesoscale Variability, Sea Level Anomalies (SLA), Eddies, Satellite Altimetry,

15. NUMBER OF PAGES
85

16. PRICE CODE

17. SECURITY CLASSIFICATION OF REPORT	18. SECURITY CLASSIFICATION OF THIS PAGE	19. SECURITY CLASSIFI- CATION OF ABSTRACT	20. LIMITATION OF ABSTRACT
Unclassified	Unclassified	Unclassified	UL

NSN 7540-01-280-5500

Standard Form 298 (Rev.289)
Prescribed by ANSI Std. 239-18

Approved for public release; distribution is unlimited

STRUCTURE AND VARIABILITY OF THE MESOSCALE CIRCULATION IN THE CARIBBEAN SEA AS DEDUCED FROM SATELLITE ALTIMETRY

Luis Pibernat
Lieutenant Junior Grade, Venezuelan Navy
B.S., Venezuela Naval Academy, 1991

Submitted in partial fulfillment of the
requirements for the degree of

MASTER OF SCIENCE IN METEOROLOGY AND PHYSICAL OCEANOGRAPHY

from the

NAVAL POSTGRADUATE SCHOOL
June 1998

ABSTRACT

Four years of Topex/Poseidon (T/P) and European Remote Sensing Satellite (ERS) altimetry data in the Caribbean Sea are used to describe the structure and variability of the mesoscale circulation in this area. These results are compared with satellite-derived sea surface temperature (SST) and drifter trajectories for the same period of time. Contour maps of sea surface height anomalies made for each 10-day period (T/P data) reveal the formation and evolution of anticyclonic and cyclonic mesoscale features in the central part of the Caribbean Sea during the entire period studied. These features move westward at average speeds between 10 and 15 cm/s, growing in amplitude up to 25 cm. Also, a quasi-permanent gyre is detected in the Golfo de los Mosquitos (coast of Panama and Colombia). The sense of rotation of this gyre is shown to be modulated seasonally. Enhanced relative clockwise and counterclockwise rotation are observed during the rainy season (June-October) and the dry/windy season (January-April), respectively. No strong mesoscale anomalies are detected in the eastern part of the Caribbean Sea where they are expected. A seasonal cycle is found in the sea level anomaly (SLA) derived from T/P and ERS-1 data due to steric effects. Upwelling is observed near the coast of Venezuela during the dry season. A comparison of SLA with SST is made and good correlation is observed at some locations. Drifter trajectories contemporaneous with SLA data agree well with the sense of rotation of strong features, but the drifter speeds are twice the absolute geostrophic currents calculated from SLA.

TABLE OF CONTENTS

I. INTRODUCTION 1

II. BACKGROUND 3

A. BASIN DESCRIPTION 3

B. OCEANOGRAPHY OF THE CARIBBEAN SEA 5

III. DATA AND METHODS 15

A. SATELLITE ALTIMETRY 15

B. ALTIMETER MEASUREMENTS AND CORRECTIONS 23

C. PRECISE ORBIT DETERMINATION 27

D. SEA LEVEL ANOMALIES 28

E. METHODOLOGY 33

IV. RESULTS AND DISCUSSION 39

A. COMPARISON ERS-1 AND TOPEX/POSEIDON (T/P) 39

B. COMPARISON T/P AND SST 40

C. QUALITATIVE DESCRIPTION OF MESOSCALE FEATURES 46

D. QUANTITATIVE DESCRIPTION OF MESOSCALE FEATURES 55

E. COMPARISON OF T/P WITH DRIFTERS 60

V. CONCLUSIONS 65

VI. RECOMMENDATIONS 67

LIST OF REFERENCES 69

INITIAL DISTRIBUTION LIST 73

ACKNOWLEDGMENTS

I want to acknowledge the Archiving, Validating and Interpreting Space Oceanography (AVISO) Data who supplied the T/P and ERS-1 SLA data sets. "The SLA products were supplied by the CLS Space Oceanographic Division, Toulouse, France (AVISO/Altimetry, 1996; Le Traon et al., 1995). The ERS products were generated as part of the proposal "Joint analysis of ERS-1, ERS-2 and TOPEX/POSEIDON altimeter data for oceanic circulation studies" selected in response to the announcement of opportunity for ERS-1/2 by the European Space Agency (Proposal code: A02.F105)." cited from AVISO, 1997.

I would like to extend profound thank and deep appreciation to my thesis advisor, Dr. Pierre-Marie Poulain, who was willing to work with me on the Caribbean Sea. His guidance and patience were invaluable and made me learn a tremendous amount in a very short period of time. In addition, I want to thank Dr. Newell Garfield, my second reader, for his advice.

I want to thank Dr. Tokmakian who handed the data sets distributed by AVISO to us and made this work possible. My gratitude goes to Dr. Olson of the University of Miami, who provided the drifter data set, and the Jet Propulsion Lab (JPL), who provided the satellite-derived SST data set. Both data sets were very important in the elaboration of this work. Also, I want to thank Mike Cook, who helped me with the MATLAB codes used in this work. I would like to express my sincere thanks to the Faculty of the Departments of

Oceanography and Meteorology for the knowledge offered to me during these two years of studies at the NPS.

I also want to express my gratitude to my classmates of the U.S. Navy and other countries for their support and friendship. I feel lucky for the opportunity of meeting them during my time at the NPS.

Finally, I would to thank God for helping me to overcome with success one more stage in my life and my military career. Special thanks go to my family and friends for their support and words of encouragement; to the Venezuelan Navy for giving the opportunity to attend NPS; and specially to my girlfriend Monica Garcia, whose love, support and understanding were always my inspiration during the course of this challenging journey.

I. INTRODUCTION

The oceanography of the Caribbean Sea is of great importance because it has a fundamental role in the formation of the Gulf Stream system and, consequently, the circulation of the North Atlantic. The currents of the Caribbean Sea have strong temporal and spatial scales of variability (Molinari et al., 1981). The near surface dynamics govern the formation and dissipation of mesoscale variability in the area (eddies and meanders), as well as coastal upwelling. Previous studies of the surface currents in the Caribbean Sea were based on shipboard measurements of dynamic topography (Gordon, 1967); satellite-tracked drifting buoys (Molinari et al, 1981; Kinder, 1985); and numerical models (Heburn et al., 1982; Thompson et al., 1992).

In the past decade satellite altimeters have confirmed the ability to detect ocean dynamic features in the mesoscale range. Consequently, our knowledge about mesoscale features on the global oceans has been improved by the use of satellite altimetry. Nystuen and Andrade (1993) observed sea surface height variability around ± 25 cm in the Caribbean Sea using GEOSAT altimetry data collected between 1987-1988.

The present study provides more detailed descriptions of the structure and variability of the mesoscale circulation in the Caribbean Sea using Topex/Poseidon (T/P) and European Remote Sensing Satellite (ERS) altimetry data between October 1992 and October 1996. Previous studies have suggested that mesoscale circulation features are prevalent in this area and the expectation is that T/P or ERS resolution is accurate enough to detect such features.

This thesis is divided into five chapters. Chapter II reviews the geography and oceanography of the Caribbean Sea. A review on satellite altimetry, altimeter measurements, corrections applied to them, and precise orbit determination is presented in Chapter III. Sea Level Anomalies (SLA) and the methodology used in this thesis are also discussed in Chapter III. In Chapter IV the main results are presented and discussed. T/P data are compared to ERS, to satellite-derived SST data, and to drifter observations. The mesoscale circulation features in the Caribbean are described qualitatively and quantitatively using T/P SLA maps. In Chapter V, the conclusions derived from this work are presented. Finally, we make some recommendations to be used in future similar work in Chapter VI.

II. BACKGROUND

A. BASIN DESCRIPTION

The Caribbean Sea is an extension of the Atlantic Ocean with about 2,000,000 square kilometers in area, which forms a semi-enclosed basin on the western North Atlantic Ocean. It is limited to the south by South America (Venezuela and Colombia), to the west by Central America from Colombia to the Yucatan Peninsula, to the east by a group of small islands known as the Lesser Antilles and to the north by the Greater Antilles (Cuba, Jamaica, Hispanola Island and Puerto Rico; see Fig. 1). This complicated geography suggests complexity and extensive mesoscale variability (scale ~ 100 km) of the water circulation that should make the Caribbean an interesting focus of study.

The bottom topography of the Caribbean Sea shows a succession of five basins, separated by sills of depth of less than 2000 m and set apart from the main Atlantic basin by an arc of islands that contain several passages with sill depths between 740 and 2200 m (Tomczak and Godfrey, 1994). Together with the Gulf of Mexico, the Caribbean Sea is often considered as the American Mediterranean Sea. The main geography of the Caribbean Sea is shown in Fig. 1; and its bottom topography and general circulation are shown in Fig. 2. From right to left, the Grenada Basin is located between the Lesser Antilles Arc and the Aves Swell or Ridge; the Beata Ridge separates the Venezuelan Basin and the Colombian Basin. Between the Colombian Basin and the Cayman Basin is the Jamaica Ridge, which extends to the southwest forming the Nicaraguan Rise. Finally, the Yucatan basin is separated from the Cayman Basin by the Cayman Ridge and ends in the Yucatan Strait.

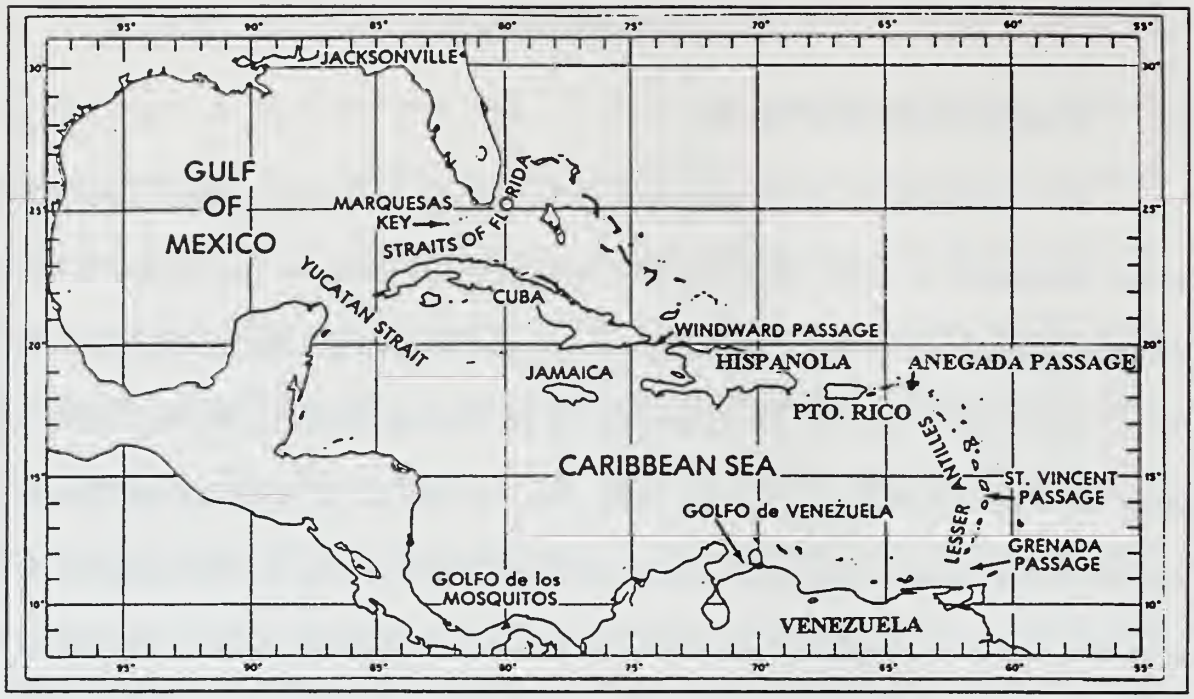

Figure 1. Geography of the Caribbean Sea and the Gulf of Mexico (after Kinder, 1983)

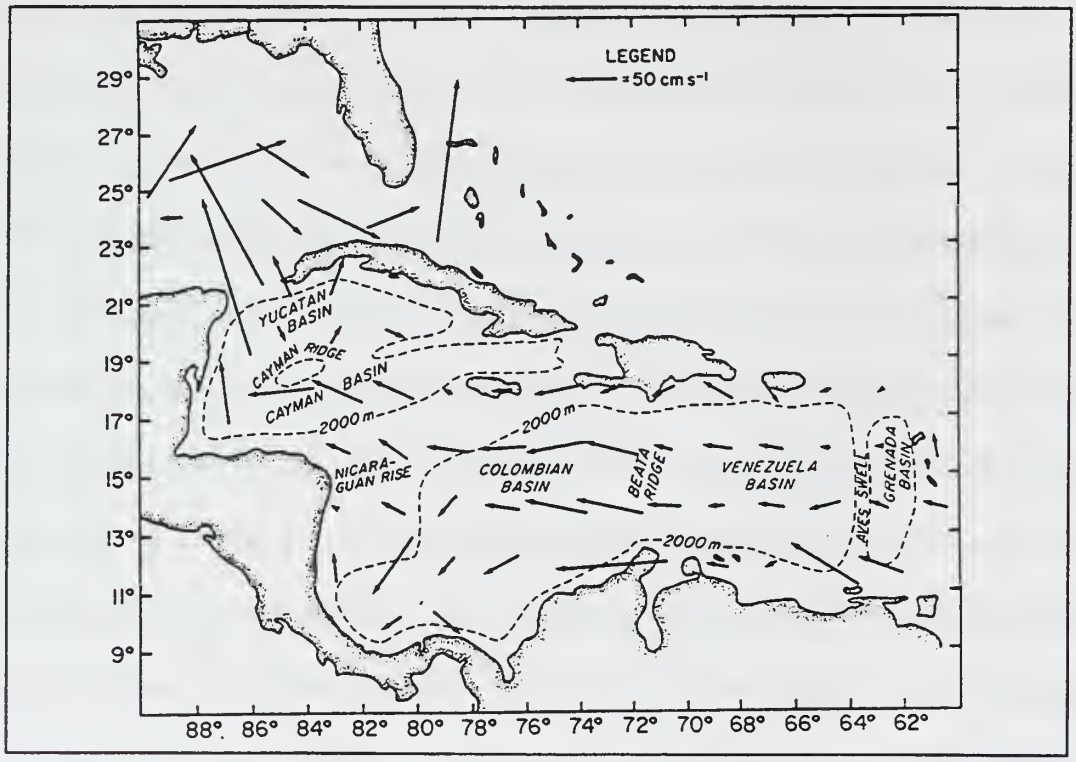

Figure 2. Caribbean Sea bottom topography and general circulation (from Molinari et al., 1981)

B. OCEANOGRAPHY OF THE CARIBBEAN SEA

The oceanography of the Caribbean Sea has been studied since the beginning of this century. Wust (1963; 1964) and Worthington (1955; 1966) discuss the deep water structure of the Caribbean. In these studies it was shown that the Caribbean Sea water structure is highly stratified in the upper 1200 m, weakly stratified between 1200 m and 2000 m and nearly homogeneous below 2000 m. Therefore, the water structure is mainly controlled by the sill depths between the island arcs.

Wust (1964) and Morrison and Nowlin (1982) described the distribution of water masses in the Caribbean Sea using a series of easily identifiable layers. Each layer derives its characteristic properties from water masses of individual origin. The following water masses were recognized in the area: (1) Subtropical Underwater, characterized by the salinity maximum found at 150-200 m, enters the Caribbean from the east through passages in the Lesser Antilles; (2) Caribbean Surface Water, a combination of Amazon River Water and local freshwater runoff from South America, is found at depths of 100-150 m; (3) Sargasso Sea Water, characterized by the oxygen maximum at depths of 200-400 m, enters through the passages in the Greater Antilles; (4) Tropical Atlantic Central Water, characterized by the dissolved oxygen minimum at depths of 400-600 m, and Antarctic Intermediate Water, characterized by the salinity minimum at depth of 600-900 m, both enter mainly through the southern passages in the Lesser Antilles. Finally, (5) North Atlantic Deep Water, characterized by a silicate minimum at depth of 1600-1800 m, enters the Venezuela basin through the Anegada Passage and the Colombian Basin through the channel between Jamaica and Hispanola (Fig. 1).

The dynamics of the deep water is discussed in several works. Wust (1963; 1964) presented an analysis based on all available data at that time (i.e., 1725 hydrographic stations from oceanographic cruises) to describe the deep circulation of the water masses in the basins of the Caribbean Sea. It was shown that the deep and bottom waters in this area are renewed principally through the Anegada and Windward Passages, although the nature of the bottom water renewal is controversial; see, e.g., Sturges (1965) or Wust (1964) for more details. On the other hand, Worthington (1955; 1966) suggested that no renewal of the bottom water has occurred in recent times and that a slow warming of the Caribbean bottom water is presently occurring. More recently, Froelich and Atwood (1974) and Atwood et al. (1979) were able to show that the renewal process is still taking place from measurements of the deep silicate content in the area.

Wust (1963; 1964) made the first attempt to describe the surface dynamics using extensive long-term averages of ship drift observations to represent the mean monthly surface currents. In general, the main feature of the surface circulation is the Caribbean Current, which is oriented along the main east-west axis of the sea (Fig. 3). Water from the Atlantic Ocean generally enters the Caribbean through the various passages among the islands of the Greater and Lesser Antilles and generally exits through the Yucatan Strait.

Most of the water that enters the Caribbean region comes from the confluence of the North Equatorial Current and the Guiana Current, which flows generally to the northwest along the continental shelf of South America (Fig. 3). The water of the Guiana Current is generally affected by the river runoff of the Amazon and Orinoco rivers. The

confluence flow divides into two currents, the Antilles Current that flows along the Atlantic side of the West Indies and the Caribbean Current that flows to the west through the Caribbean basin and exits to the Gulf of Mexico through the Yucatan Strait. The water of the Caribbean Current eventually reaches the Florida Strait and becomes part of the Gulf Stream. The contribution of the Caribbean Current to the volume transport of the Gulf Stream is important, and, according to Metcalf (1976), it accounts for over 50 % of

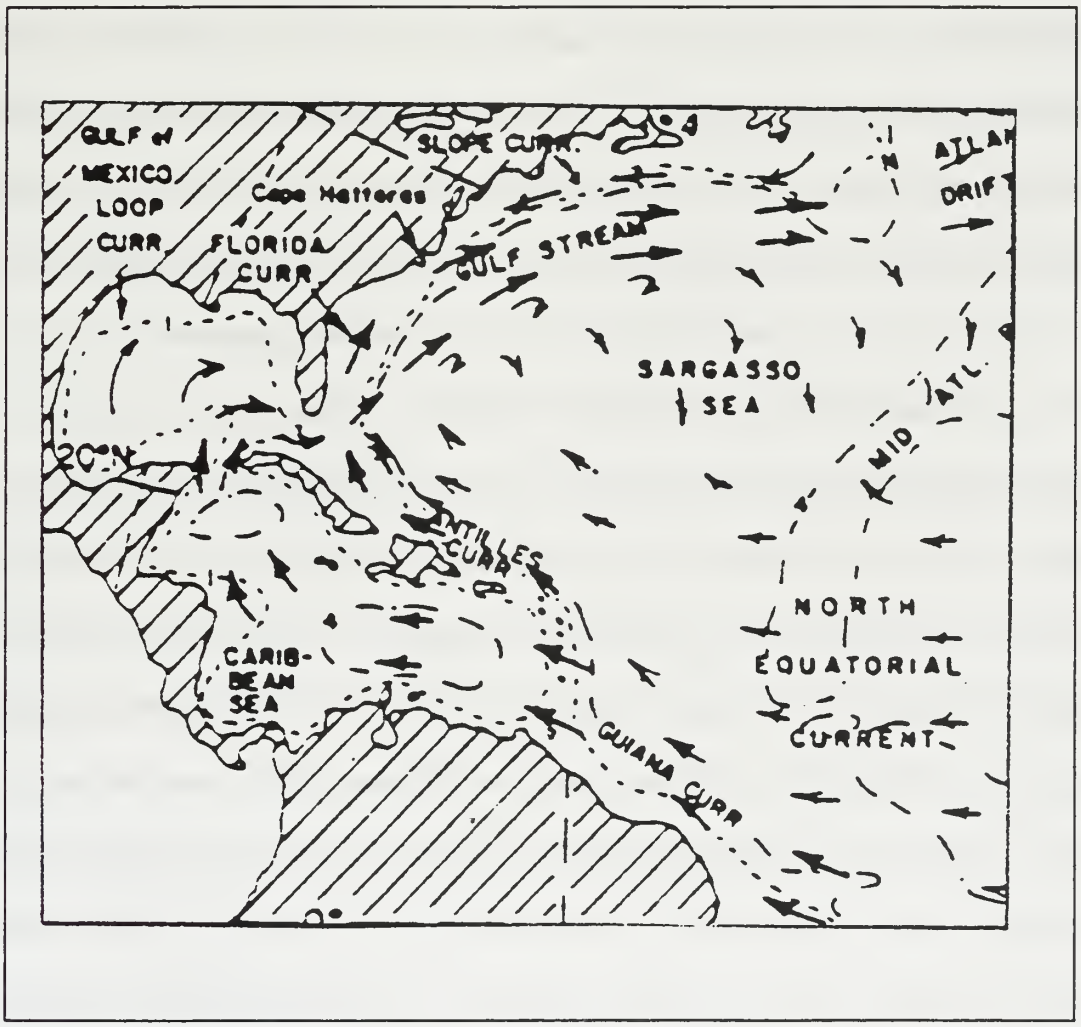

Figure 3. Surface circulation of the North Atlantic Ocean (after Pickard and Emery, 1990)

the volume of the Gulf Stream off Cape Hatteras; and between 20 to 25% of the maximum volume transport of that current.

Gordon (1967) described the surface circulation of the Caribbean Sea using six north-south hydrographic sections across the basin that were collected over a span of several years. The classical geostrophic method was used to estimate the velocities and transports. Gordon (1967) described the axis of the Caribbean Current to be located approximately 200-300 km north of the coast of South America at about latitude 15° N. His calculations of the volume transport gave an average of 31 Sv toward the west. Maps of surface dynamic topography from Gordon (1967) show gyres in the western Caribbean and suggest the presence of a countercurrent along Costa Rica and Panama, which ends on the Colombian coast. This flow is usually called the Darien Countercurrent. Also, a counter flow along the coasts of Cuba and Hispanola islands was observed.

Continuing with indirect techniques, Roemich (1981) used an inverse method to make a calculation of the geostrophic flow by applying mass and salt conservation. His estimation of the total transport flowing through Yucatan Strait was 29 Sv, of which 22 Sv came from the east flowing across the Caribbean and 7 Sv came from the north via Windward Passage into the north Cayman basin. The inverse method demonstrated an ability to resolve large features of the circulation. The geostrophic flow was described in the following way: near the Venezuelan basin the flow seems to separate into several streams and eddies; then over the southern part of the Colombia Basin, the Caribbean Current becomes broad and suggest the presence of a recirculation flow near Jamaica.

The circulation described by Wust (1964), Gordon (1967) and Roemmich (1981) described many aspects of the main flow that can be summarize as a westward flow with speeds of 0.5 to 1.0 m/s becoming stronger in the southern Caribbean and the Strait of Yucatan. They were unable to study temporal or spatial variability in any detail. More recent hydrographic and direct current measurements showed temporal variability on scales from 12 hours to 60 days, and spatial variability on scales from 100 to 500 km (Kinder et al., 1985). Closely spaced hydrographic stations have shown mesoscale variability as eddies and meanders with roughly 100 km in diameter. Another attempt to directly trace Caribbean current patterns was by the use of drift-bottles. Results can be found in Brucks (1971), Duncan et al., (1977) and Metcalf et al., (1977). These results agree with previous ideas regarding the circulation and introduce zones of strong variability. However, the confidence of such data is questionable.

Another way to study the circulation pattern in the Caribbean Sea is by using drifting buoys that report their positions by satellite. These buoys help to increase the knowledge about spatial variability in the Caribbean Sea. Molinari et al., (1981) observed the surface currents using 19 satellite-tracked drifting buoys released in the eastern Caribbean during 1975-1976. The result of this work suggested that mesoscale variability in the surface currents is important across the Aves Swell or Rise, Beata Ridge, and Nicaraguan Rise, as shown in Fig. 4. Large eddies and meanders in the vicinity of these areas suggested that the large topographic features of the Caribbean Sea may be an important source of the mesoscale variability in the basin. It was deduced that the westward flowing current interacts with these ridges forming eddies or meanders. Also, it

was shown how the Caribbean Current intensifies 200 km to the north of the coast of Colombia (speeds greater than 80 cm/s), as well as south of the Nicaraguan Rise (speeds approaching 80 cm/s) and south of the Yucatan Strait. Another important feature revealed by the drifting buoys is the clockwise circulation gyre in the Golfo de los Mosquitos.

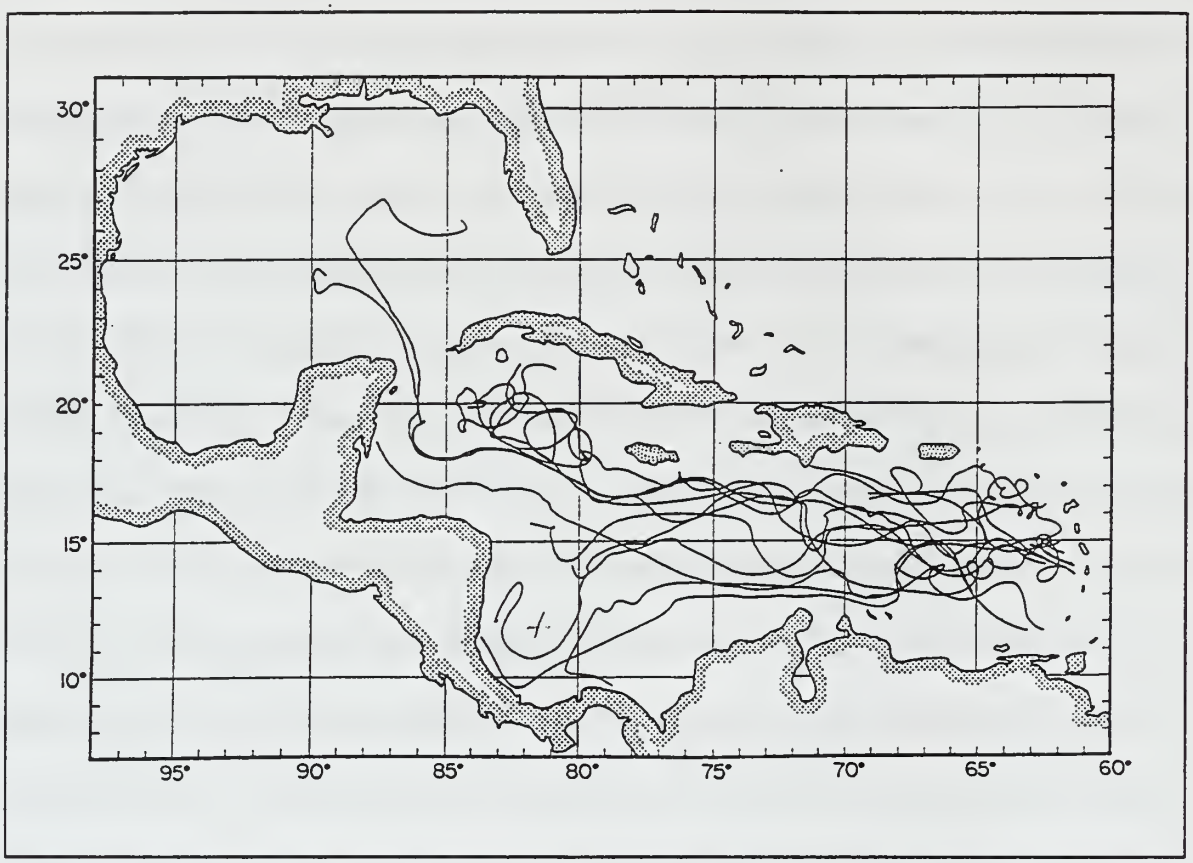

Figure 4. Trajectories of satellite-tracked drifting buoys in the Caribbean (from Molinari et al.,1981)

Another drifter study was done by Kinder (1983). In this case, four satellite-tracked drifters (Fig. 5) were deployed near the southern Lesser Antilles in fall 1977. This study can be considered as a supplement to the information collected by Molinari et al., (1981). Even though the drifters use by Molinari et al., (1981) had shallower drogues (30

m instead of 100 m), both studies show similar characteristics of the surface velocities. Bottom topography and winds were rejected as the primary reason of the mesoscale variability; but local wind forcing was mentioned as a possible reason to modify the variability. The cause of meanders and eddies was suggested to be the inherent instabilities of the currents in the Caribbean. Kinder (1983) tabulated typical speeds of 20 cm/s in the Grenada Basin, 50 cm/s inside the Caribbean Current across the southern Venezuela and Colombia Basins and 80 cm/s near the Yucatan Strait. Finally, the drifters showed a counterclockwise circulation in the Golfo de los Mosquitos. It was strongly suggested that an eddy often appear in this area, but that it can be either cyclonic or anticyclonic.

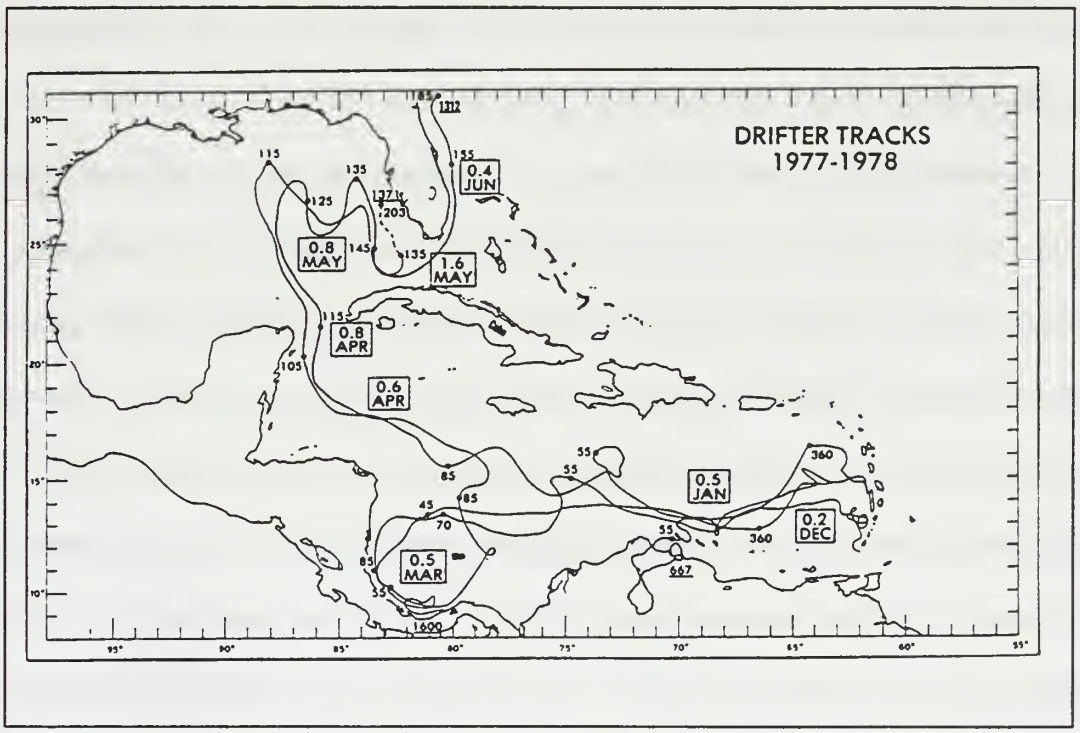

Figure 5. Trajectories of satellite-tracked drifters in the Caribbean Sea (from Kinder, 1983)

Heburn et al. (1982) investigated the circulation in the southeastern Caribbean with an eddy-resolving numerical model. Regardless of the bottom topography, it was demonstrated that eddies form there. Also, the model replicated drifter behavior in the southeastern Caribbean without the use of wind forcing. It was suggested that the mesoscale features are caused by inherent instabilities in the Caribbean Current. More recently, a primitive equation model of the sea surface dynamic height in the Caribbean Sea by Thompson et al. (1992) verified most of the large features of the circulation described here. It also indicated a well-established cyclonic eddy in the southwestern portion of the Colombian Basin (Golfo de los Mosquitos). The same eddy location was confirmed by a global eddy resolving circulation model by Semtner and Chervin (1992). In this case the eddy showed a strong seasonal intensification with a maximum in November-February and a minimum in June-July.

Nystuen and Andrade (1993) used data from the Geosat Exact Repeat Mission (ERM) altimetry collected during 1987-1988 to track mesoscale ocean features in the Caribbean Sea. Two anticyclonic features were found during April-July of each year that propagate westward with average speeds of 15 cm/s. No mesoscale features were evident during any other seasons. Also, a quasi-permanent cyclonic eddy in the Golfo de los Mosquitos was described, confirming model predictions. Anomalies in the eastern part were expected because previous work (Molinari et al., 1981; Kinder et al., 1985; Morrison and Smith, 1990) had suggested the existence of mesoscale features in this area; however, anomalies were not detected. The reason for that was suggested to be the quasi-permanent characteristic of these features in the eastern part of the Caribbean Sea.

Carton and Chao (1998) examined T/P data and a 1/6° Atlantic Ocean model simulation to study the Caribbean Sea eddies. They found similarities in the SLA observed from T/P and simulated using the model, with maximum SLA values in the west. They believe that anticyclonic eddies originate in the North Brazil retroflection that interacts with the topography of the islands of Trinidad and Tobago, creating cyclonic and anticyclonic eddies at the eastern Caribbean Sea. Then, these eddies move with the Caribbean Current and at some point interact with it. This is a hypothesis suggested by the simulation of the model, and need further comparison with results from other model simulations at higher spatial resolution.

There are two major factors that can generate available potential energy in the oceans: the wind stress and thermohaline effects. Gordon (1967) stated that the Caribbean area does not have strong thermohaline effects because the Caribbean Sea lacks the temperature extremes, and precipitation exceeds evaporation in almost all the area. Thus, the major source of energy in the Caribbean Sea is derived from the wind. Wust (1964) stated that the driving force of the surface currents of the Caribbean Sea are the Northeast Trade Winds, which come from the northeastern and eastern sections of the Caribbean.

The climate of the Caribbean region is characterized by two tropical seasons. A dry or windy season from December to April, and a humid or rainy season from June to October. The rest of the year is considered to be transitional, moving from one season to another (Andrade, 1991). The seasonal movement of the Intertropical Convergence Zone (ITCZ) dominates the climate pattern. During the dry season, the ITCZ is located over South America, resulting in relatively uniform strong Trade Winds over the Caribbean

region. These winds cause strong upwelling along the coast of Venezuela and Colombia. On the other hand, during the humid season the ITCZ moves to the north becoming located in the middle of the Caribbean Sea. The winds die down while clouds associated with the ITCZ cause heavy rainfall that may modify the salinity and density, and consequently affect current flow. The transition period is mainly characterized in the western Caribbean by a slow change in wind direction and a lower wind speed over the entire basin.

The wind stress is the primary energy source for the surface currents. Kinder et al. (1985) and Morrison and Smith (1990) stated that the winds are stronger in the wintertime (dry season), but the magnitude of the wind stress curl is greater in the summer (rainy season). They found the maximum regional wind stress curl during July and the minimum during October. Nystuen and Andrade (1993) showed that the volume transport is positively correlated to the seasonal wind stress curl throughout the Caribbean Sea. Morrison and Smith reported an absolute maximum transport of 31.1 Sv in July and an absolute minimum of 8.2 in October, with a relative maximum in January and a relative minimum in March. All transports are westward. An apparent similarity between the transport estimates and the regional climatological wind-stress curl was shown.

III. DATA AND METHODS

A. SATELLITE ALTIMETRY

Satellite altimetry offers the possibility to measure globally sea surface heights. In order to determine the sea surface height with an altimeter, one must complete a four-step process. It begins by using a radar altimeter to measure the distance between the satellite and the sea surface. This measure is also known as the altimeter range. The next step is to compute the location of the satellite at the precise moment of measurement with respect to the reference ellipsoid. Once these two parameters are determined the atmospheric, environmental and instrumental corrections are calculated and applied to the altimeter range. Finally, the sea surface height is calculated by subtracting the corrected altimeter range from the exact position of the satellite. A high level of accuracy is required for the altimeter range and for all the correction terms in order to study the ocean currents because most of them correspond to sea surface height variations of 5-10 cm.

For oceanographic applications the sea surface height should be measured over the geoid. The geoid is the equipotential surface at mean sea level, that is, if the ocean were everywhere in stationary equilibrium relative to the earth (i.e., with no currents), its surface would define the geoid. The height of the ocean surface above or below the geoid contains information about ocean currents or tides. The form of the earth is almost regular, and can be defined in general as an ellipsoid. Because of uneven mass distributions within the earth, the true geoid deviates in height from the ellipsoid used as reference by a distance of order 50 m.

In order to determine the sea surface height relative to the geoid, it is necessary to know the shape of the geoid relative to the ellipsoid to the same accuracy as the satellite measurement. The distance measured by the satellite relates the sea surface height to the satellite orbit. The satellite orbit must therefore be determined relative to the reference ellipsoid. This involves both the modeling of the satellite orbit and the use of methods of satellite tracking and position fixing, e.g., Global Position System (GPS), Laser Retroflector Array (LRA), etc. Figure 6 illustrates the different parameters that contribute to the altimetry signal measured by the satellite.

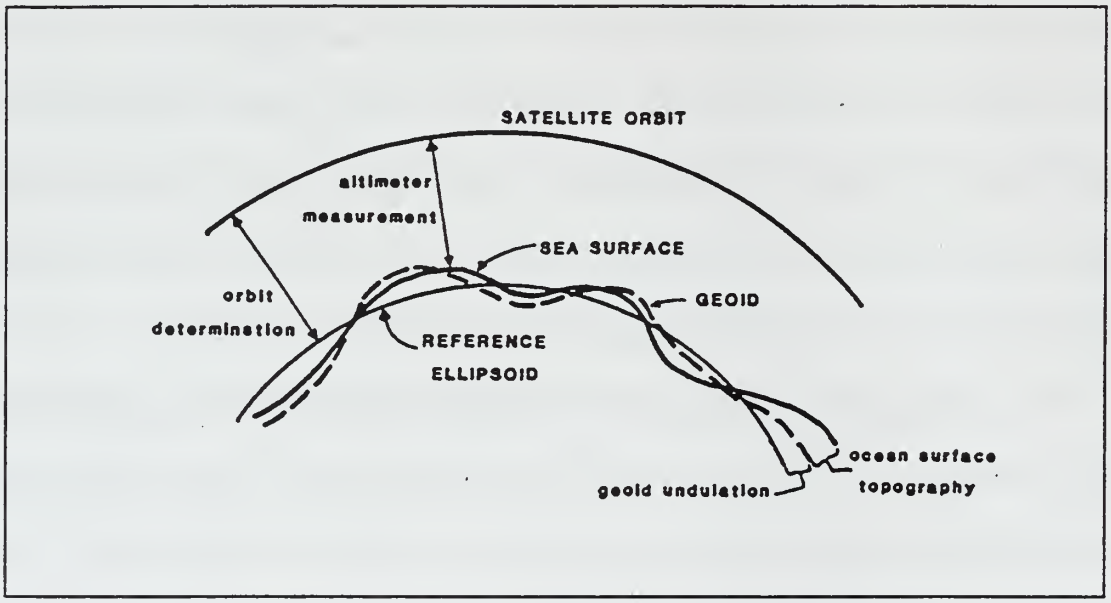

Figure 6. Parameters involved in the sea surface height measurement (from Robinson 1985)

Before continuing, a brief history about the evolution of satellite altimetry is presented. Satellite altimetry began with an experiment during the National Aeronautics and Space Administration (NASA)'s SKYLAB mission in 1973. This experiment demonstrated the feasibility of using satellite altimetry for oceanography. In 1975, NASA

GEOS-3 was launched, becoming the first satellite with an altimeter. It measured the sea surface height during 1975-1978. The data from this mission were capable of resolving only the largest features because it had large errors in orbit determination. In August 1978, SEASAT was launched and became the first oceanographic remote sensing satellite. Data from this mission were more accurate than its predecessor GEOS-3 and orbit determination was improved. Unfortunately, SEASAT suffered a fatal failure after 3 months and no further data were obtained.

In March 1985, the U.S. Navy's Geodetic Satellite (GEOSAT) was launched. Its primary mission was to improve knowledge of the marine gravity field or the geoid. This mission was accomplished after 18 months and the data resulting from it were classified by the U.S. government. Many believe that this data set is unique in terms of spatial resolution and equatorial crossing (less than 5 km). Beginning in October 1986, GEOSAT was maneuvered to a different orbit very close to the original SEASAT orbit. This part of the mission is known as the GEOSAT Exact Repeat Mission (ERM) and it had a nominal period of 17 days. This satellite remained in this orbit until its failure in January 1990.

In July 1991, the European Space Agency (ESA) launched its first radar altimeter sensor on the European Remote Sensing Satellite (ERS-1). This satellite worked in different orbit configurations. After the commissioning phase was completed (phase A), the satellite mission was sub-divided in the following phases: a three-day repeat orbit for the first ice-phase (phase B); a 35-day repeat orbit for the first multi-disciplinary phase (phase C); a three-day repeat orbit for the second ice phase (phase D); two 168-day repeat

orbit for the geodetic phases (phases E and F); and finally another 35-day repeat orbit for the second multi-disciplinary phase (phase G) that also was used for the calibration and validation of the new ESA satellite, ERS-2. During the 35-day repeat orbits, the equatorial track spacing was reduced to 39 km (see Fig. 7).

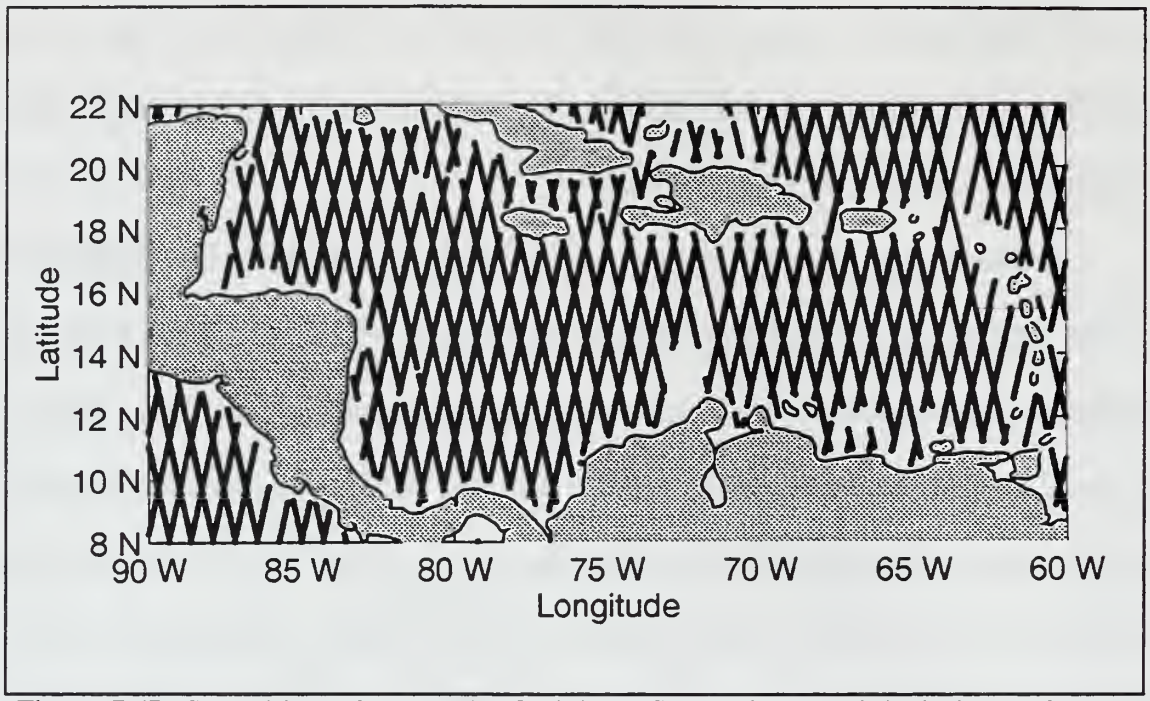

Figure 7. ERS-1 orbit tracks over the Caribbean Sea during multidisciplinary phase

The radar altimeter on board ERS-1 is a Ku-band (13.8 GHz) nadir-pointing active microwave sensor designated to measure the time return echoes from ocean and ice surfaces. It has two operational modes, ocean (bandwidth 330 MHz) or ice (bandwidth 82.5 MHz). The radar altimeter provides accurate measurements of sea surface elevation, significant wave heights, sea-surface wind speeds and various ice parameters. Other instruments on board the ERS-1 satellite are: (1) An active Microwave Instrument (AMI) combining the functions of a Synthetic Aperture Radar and a Wind Scatterometer; (2) An Along-Track Scanning Radiometer (ATSR) and Microwave

Sounder (MW) combining infrared and microwave sensors; (3) A Precise and Range Rate Equipment (PRARE) for the accurate determination of satellite position and orbit characteristics; and (4) A Laser Retro-Reflector (LRR) for the satellite position and orbit using laser ranging stations on the ground. ERS-1 is still working, but the data are no longer being recorded and transmitted to ground stations. The ERS-2 satellite is similar to ERS-1, but it carries a new instrument: The Global Ozone Monitoring System (GOME), which is a nadir-viewing spectrometer to determine the atmosphere's content of ozone.

The Topex / Poseidon (T/P) satellite was launched in August 10, 1992. It was the first space mission specifically designed and conducted for studying the ocean's circulation. The mission was conducted together by the U.S. space agency, NASA, and the French space agency, Centre National d'Etudes Spatiales (CNES). The T/P satellite is orbiting the earth at an altitude above ground of 1336 km with an inclination of around 66 degrees, an equatorial cross-tracks separation of 316 km (see Fig. 8), and a near 10-day repeating orbit (exact period is 9.916 days). It has two different altimeters: The NASA altimeter, referred to as TOPEX, is a dual-frequency radar altimeter that transmits at 13.66 GHz and 5.36 GHz (Ku/C-band). The design is based on previous altimeters with significant improvements. The two frequencies are used to provide more accurate atmospheric propagation correction. The CNES altimeter, known as POSEIDON, is a solid-state Ku-band (13.65 GHz) altimeter. It is an experimental sensor, which requires less power and weighs less than the NASA altimeter. Both altimeters share the same antenna and cannot operate at the same time. TOPEX operates during almost 90% of the time and POSEIDON operates during the rest of the time (Fu et al., 1994).

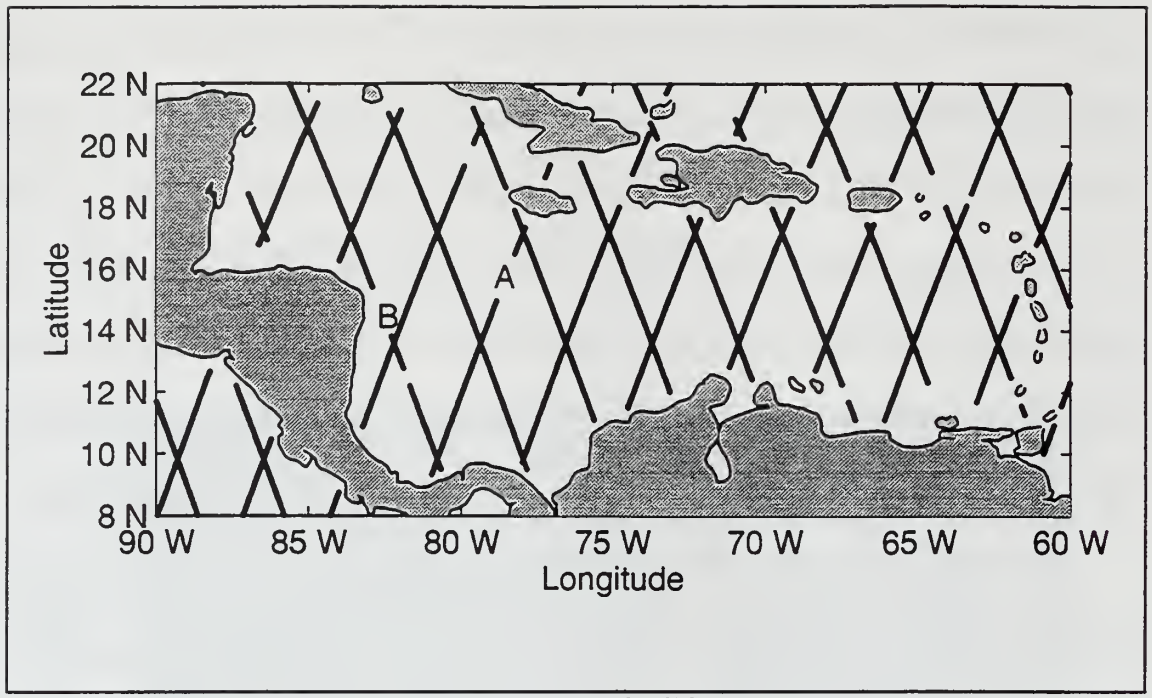

Figure 8. Topex/Poseidon orbit tracks over the Caribbean Sea. Tracks A and B are used for contouring height anomaly time series.

Other sensors on board of the satellite are: the TOPEX microwave radiometer (TMR), a Laser retroreflector array (LRA), a Doppler orbitography and radiopositioning integrated by satellite (DORIS) dual doppler tracking system receiver, and the Global Positioning System (GPS) demonstration receiver. The TMR is used to estimate the total water content in the atmosphere using three frequencies (18, 21 and 37 GHz) to later apply the respective correction on the travel time. The other three sensors are use for tracking the exact position of the satellite. The LRA uses a global network of laser ranging stations; the DORIS receiver also uses a network of ground transmitting stations to track the satellite using microwave Doppler techniques; and the GPS demonstration receiver uses the network of satellite GPS and several receivers in Earth for continuous tracking of the satellite's position. The precise orbit determination of the T/P satellite is

one of the reasons of the success of this mission (Fu et al., 1994). The T/P measurement system is shown in Fig. 9.

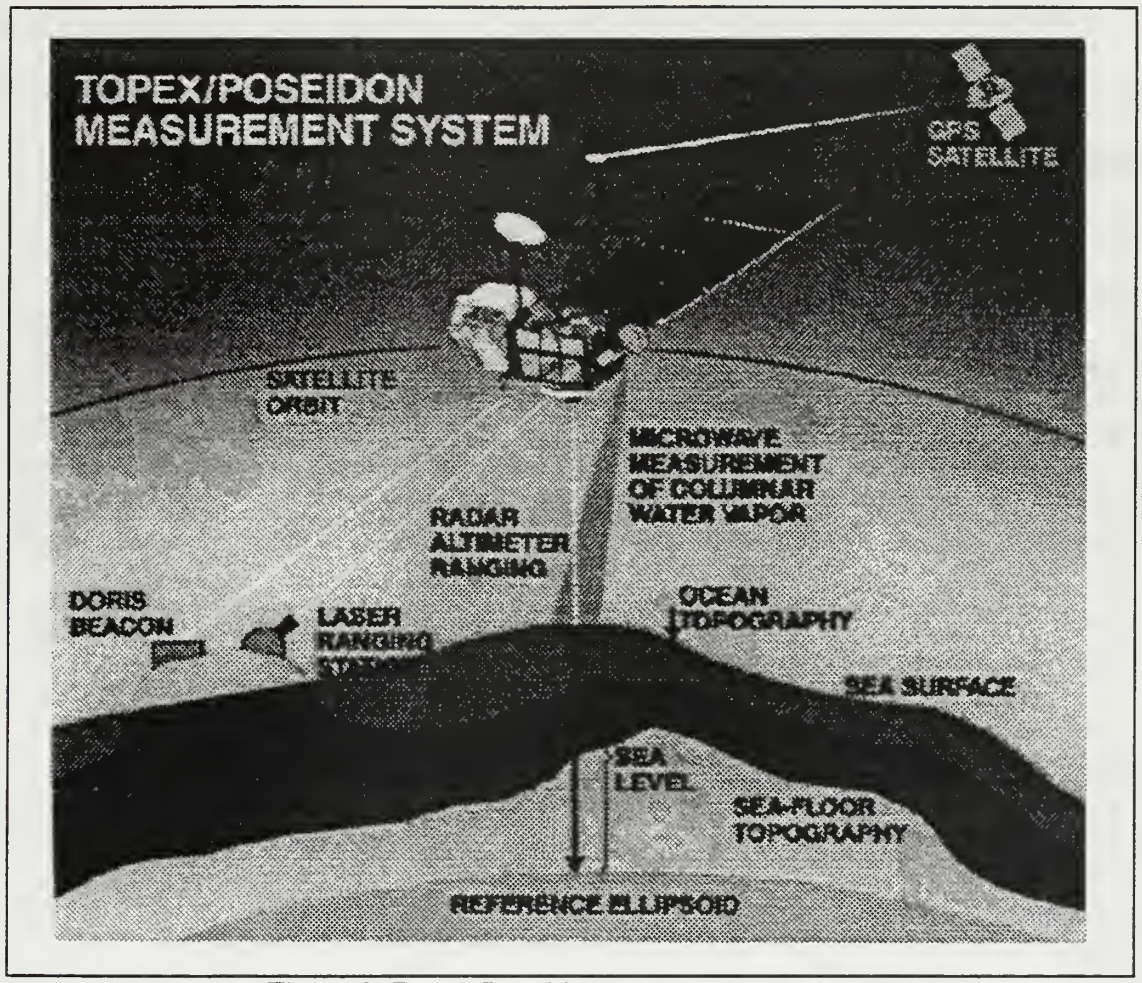

Figure 9. Topex/Poseidon measurement system.

Satellite control and data processing are conducted by Jet Propulsion Laboratory (JPL) at Pasadena, California. CNES has implemented an Information Processing Center at Toulouse, France for the sensor control and data processing of its instruments via an interface with the mission operations control center in JPL. NASA and CNES are processing Geophysical Data Records (GDR) for their respective altimeter measurement. The NASA GDR is refer as GDR-T and the CNES GDR is refer as GDR-P. Both data

sets are combined to produce the merged GDR (M-GDR). The correction applied to satellite altimetry and the process to get the Sea Level Anomaly will be discussed in the next sections.

A summary of key information and main sources of error, for the present and past satellite missions equipped with altimeters, is shown in Table 1.

	GEOS-3	SEASAT	GEOSAT	ERS1/ERS2	TOPEX/ POSEIDON
Time of Operation	1975-1978	1978	1985-1989	1991-present	1992-present
Agency	NASA	NASA	U.S. NAVY	ESA	NASA/CNES
Orbit height (km)	843	800	800	780	1336
Inclination	115°	108°	108°	98.5°	66°
Repeat cycle orbit (days)	various	3	17 during ERM	Ice: 3 Multdic.: 35 Geodetic:168	10
Frequency (GHz)	13.9	13.5	13.5	13.8	T:13.6 and 5.3 P: 13.65
Instrument noise (cm)	50	10	5	3	< 2
EM bias (cm)	10	5	2	2	< 2
Orbit accuracy (cm)	30 - 50	30	20	18	3.5
Root-sum-squared error	67 cm	33 cm	22 cm	19 cm	< 5 cm

Table 1. Important information and main sources of error of the present and past satellite altimetry missions (after Petterson et al.,1995)

B. ALTIMETER MEASUREMENTS AND CORRECTIONS

We now explain the principle of altimeter measurements and discuss in detail the various corrections made on the raw data, with particular focus on the T/P altimeter.

The radar altimeter is a nadir-looking active microwave sensor. The signal pulse is transmitted vertically downward. It interacts with the land or ocean and is reflected back to the altimeter antenna. The time that the pulse takes for this round-trip is accurately measured and is used, together with knowledge of the propagation speed of electromagnetic waves, to compute the altitude of the antenna above the reflecting surface (altimeter range). After that, the exact position of the sensor with respect to a fixed reference surface, such as the reference ellipsoid, needs to be precisely known. The sea surface height above the same reference level can be computed subtracting the altimeter range from the exact position of the sensor.

To increase the level of accuracy, many return pulses are typically averaged to provide one data point every second along the satellite ground track. Altimeter measurements have many sources of error. Several corrections need to be applied due to instrument errors, environment, sea surface effects, tides, and satellite orbit uncertainty. A high level of precision is required for all corrections terms involved in the calculation of the sea surface height. A schematic view of the various components and corrections that are important for the sea surface height is shown in Fig. 10.

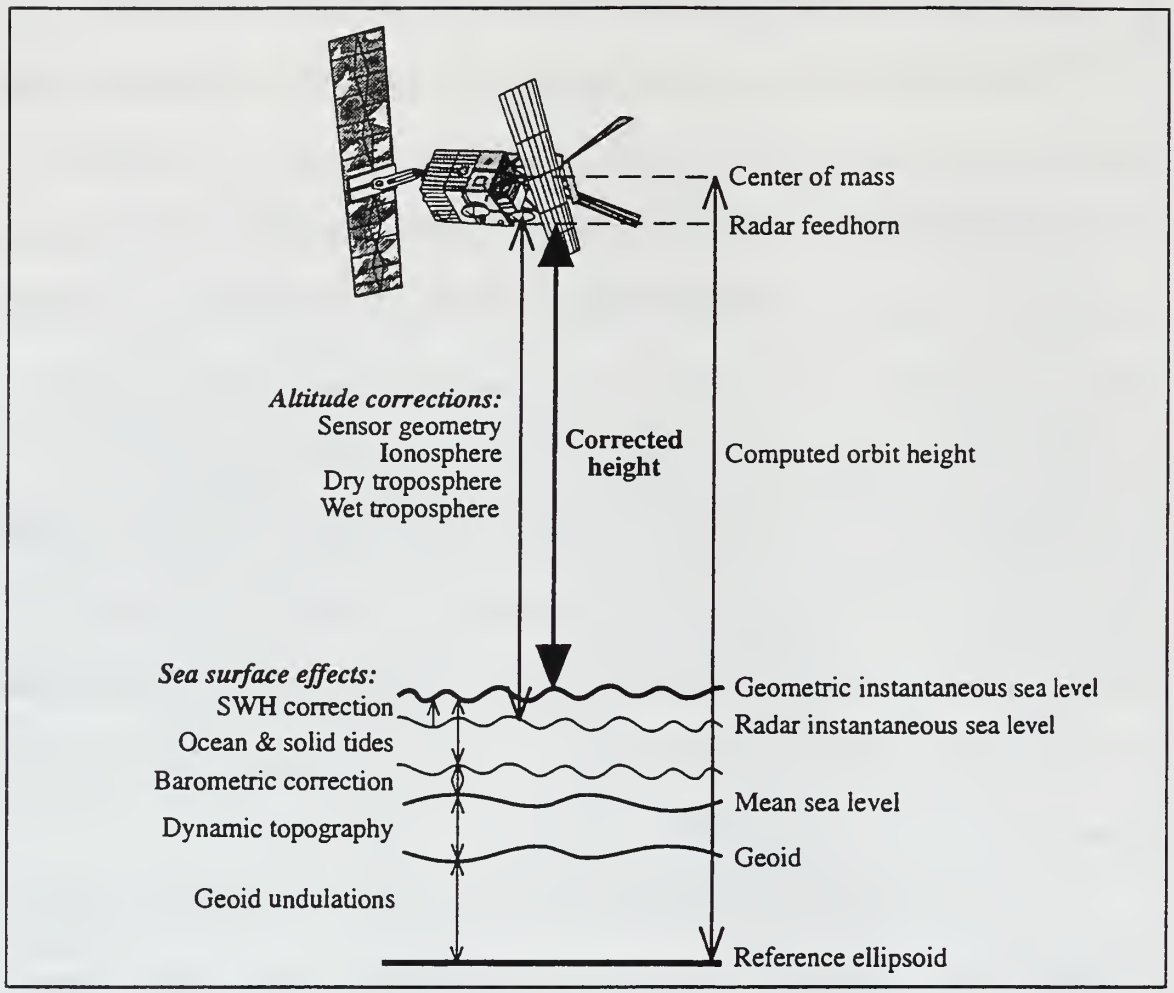

Figure 10. Various components and corrections that are important in radar altimetry (from Petterson et al., 1995)

First we discuss the sources of error related to the instruments. It is important to determine where the center of mass of the spacecraft is located and the exact location of the altimeter antenna in the spacecraft. The ability of the sensor to measure the exact arrival time of the reflected pulse, called tracker bias, needs to be considered. Another error is due to the simplified calculation performed on the altimeter waveform on board the satellite, which is known as mispointing and skewness effects. These effects are related to the sea state and altimeter pointing angle.

Second, the error and corrections related to the environment are discussed. An error arises from the fact that the troughs of ocean waves present a greater number of reflecting faces than the crest, causing a bias toward the waves troughs. This bias is called Electromagnetic bias and is usually corrected using an empirical function related to altimeter derived significant wave height. It is a contributing factor, together with modeling errors introduced by on-board processing, to the Sea State Bias (SSB).

AVISO (1997) defined the SSB as the difference between the apparent sea level as measured by an altimeter and the true mean sea level. It is a function of the significant wave height and other sea-state related parameters, and depends on radar frequency. They use the so-called BM4 formula (Gaspar et al., 1994) defined as:

$$SSB = SWH\,[a_1 + a_2*U + a_3*U^2 + a_4*SWH] \qquad (1)$$

where SWH is the significant wave height in meters, U is the wind strength in m/s, and the estimates of the 'a_i' parameters are derived from a global crossover analysis.

Third, the errors and corrections related to the atmosphere that affect the outgoing and returned pulse are discussed. The ionosphere error is due to the range delay caused by the free electrons in the ionosphere, whose count in the atmosphere varies between day and night and winter and summer, being less at night and in summer. It increases with the solar sunspot maximum. Consequently it cannot be directly predicted. This error is corrected in different ways for each altimeter in the T/P satellite. For the TOPEX altimeter, the correction is derived from the dual-frequency measurements of the altimeter; and for the POSEIDON altimeter, the correction is derived from the dual-

frequency signals received by the DORIS receiver (AVISO, 1997). This correction depends upon the level of solar activity at the time of the observation and the time of the day.

The wet troposphere error is the range delay caused by the water vapor content in the atmosphere. It is related to the total water vapor content in the column directly below the altimeter nadir path. In the Caribbean Sea, the atmospheric water vapor content is sometimes high and with high variability, especially in the ITCZ. In the past, this error was corrected using meteorological models or passive microwave radiometer data. The Archiving, Validation, and Interpretation of Satellite Data in Oceanography (AVISO) applies the correction in the T/P mission using the nadir-looking TMR. They retrieve the correction using the brightness temperatures measured in the three frequency channels of the TMR (AVISO, 1997).

The dry troposphere error is the range delay caused by the mass of dry air molecules in the atmosphere. This effect is directly proportional to the sea level pressure. The inverse barometer effect is the depression of the sea surface by the weight of the column of air resting on it. Also it is a function of the sea level pressure. AVISO estimate the correction for both of these errors using the sea level product of the European Center for Medium Range Weather Forecast (ECMWF) provided by the French Meteorological Office (FMO) (AVISO, 1997).

Tides can be defined as the periodic variation in the surface level of the oceans caused by the gravitational effect of the sun and moon. The moon causes the stronger effect. AVISO divides the correction for tides in three categories: ocean tides, solid earth

tides, and loading tides. It is assumed that the solid earth is flexible enough to respond to the same gravitational forces that generates the ocean tides. Loading tides come as a result of the interaction between the solid Earth and the fluid ocean tides. Tidal models are derived in part from the analysis of temporal variability in the ocean signal from previous altimeter missions. AVISO uses tidal models to correct the altimeter range. For the Solid Earth Tide, they use the model of Cartwright and Tayler (1971). For the ocean tide and loading tide, they use the empirical derived CSR3.0 ocean tide model developed by the University of Texas (AVISO, 1997).

C. PRECISE ORBIT DETERMINATION

Satellites are affected by many forces in space that modify their motion. Precise orbit determination is the analysis of satellite tracking data in order to model the position of the satellite at a given moment. This information is very important in radar altimetry and it has been the largest source of uncertainty for all missions prior to T/P. The position of the satellite is estimated from a global gravity field model (geoid) and knowledge of the various forces acting on the satellite. One of the goals of the T/P mission was to improve the understanding of the gravity field of the Earth in order to reach the science goals that were expected for the mission. The enhancement of the knowledge of the gravity field after the launch of T/P, and the various satellite tracking system installed, have provided the T/P mission with an accurate and precise orbit determination system that has reduced the most critical source of error in satellite altimetry. The three tracking systems are configured in the following way: the satellite laser ranging plus the DORIS

system as the reference system and the GPS demonstration receiver as an experimental receiver. AVISO uses the precise orbits from the NASA Joint Gravity Model (JGM) version 3. Given the high accuracy of T/P orbits, no orbit error correction is calculated and its orbit is used as the reference level. In the case of ERS-1, AVISO reduces the orbit error fitting the ERS-1 orbit to the more precise T/P data using a global minimization of ERS – T/P dual crossover differences (AVISO, 1997). The T/P –ERS-1 crossover differences give an estimate of the ERS-1 radial orbit error almost instantaneously, leading to a geometric evaluation of orbit error (Le Traon et al., 1995). This method provided a precise and homogeneous ERS and T/P corrected sea surface height data sets. As a result, ERS-1 orbits have an accuracy similar to T/P orbits: 2 cm rms (AVISO, 1997).

To verify the accuracy of the measurement made by the T/P altimeters, two verification sites are used. At these two sites, the distance between the satellite and the ocean is estimate from earth-based instruments. These measurements come from sea-level monitoring instruments located on Lampedusa Island in the Mediterranean Sea, and an oil production platform located off the coast of California. Measurements from these instruments are compared with those taken by the T/P altimeters, to ensure that the satellite's altimeters are functioning well and returning accurate measurements.

D. SEA LEVEL ANOMALIES

Sea level anomalies are departures of the sea surface from some long-term average. In the case of the sea level anomalies computed from T/P altimetry, the mean is

estimated either on three or four years. By comparing recorded sea levels to the average, the variability of the ocean can be observed between 10 day cycles. Positive sea level anomalies indicate more heat content; therefore, warmer waters and a deeper thermocline are expected. On the other hand, negative sea level anomalies indicate less heat content; therefore, cooler waters and a shallower thermocline are expected.

The process to calculate the sea level anomalies described in AVISO (1997) uses the following steps. First, valid data are selected through the use of quality control to validate the altimeter data and the geophysical corrections. The verification of the performance of the satellite and the instruments, and the integrity of the science data is a continuous process. For more information about the editing criteria for T/P refer to AVISO (1997).

Second, altimeter corrections as defined in the section B must be applied. As mentioned before, altimeter measurements have many sources of errors. Data need to be corrected for instrumental errors, environmental perturbations (wet and dry troposphere, ionospheric effects), the ocean wave influence (sea state bias), the tide influence (ocean tide and earth tide) and inverse barometer effect.

Third, orbit corrections are applied. Given the high accuracy of the T/P orbits, no orbit error correction is calculated for the T/P data. The ERS data are fitted to the more precise T/P data using a global minimization of ERS – T/P dual crossover differences (AVISO 1997). This provides ERS orbits with accuracy similar to T/P orbit (2 cm rms).

Fourth, the corrected sea surface height is calculated using the following relation:

'Sea Surface Height = Orbit – Altimeter Range – Corrections'

These lead to the Corrected Sea Surface Height (CORSSH) products distributed by AVISO.

Finally, the Sea Level Anomalies (SLA) are computed from several CORSSH files using the repeat-track analysis method. This method is based on typically averaging the return pulses to provide one data point every second along the satellite ground track. At a satellite ground speed of 7 km/s, each altimeter data value represents an extended area of about 7 km along ground track. The 1-second average values are the fundamental component included in the GDR and CORSSH products which are distributed to the scientific community. Then, the mean for T/P is calculated using 3 years of data from cycles 11 to 121 which covers the period between January 1993 and December 1995. The mean for ERS-1 is calculated using data from cycles 6 to 18 of the first 35-day repeat orbit covering the period between October 1992 and December 1993. This mean represents the sum of the geoid, the mean dynamic sea level, and the mean of error terms. The mean is finally subtracted from the CORSSH for each cycle to get the Sea Level Anomaly (SLA) induced by mesoscale circulation features.

Unfortunately, the technique of repeat track analysis also eliminates the time invariant component of geostrophic ocean currents, which is removed along with the geoid component. In our case the mean Caribbean Current is removed. The SLA is suitable for observing sea level variations associated with temporal varying quasi-geostrophic mesoscale surface features. This will be a limitation of altimetry until an independent geoid for oceanographic applications is available and it can be removed from

the altimeter data independently. Therefore, we will only focus on ocean features with temporal sea level variability.

Many dynamical processes in the ocean with spatial resolution of hours or longer may be considered to be in geostrophic balance in which the pressure forces driving the flow are balanced mainly by the Coriolis force. The Coriolis force is the inertial force due to the absolute acceleration that occurs as a body moves relative to a frame of reference that is itself rotating. In the ocean, with x and y coordinates in the east and north directions respectively, fixed relative to the rotating earth, and the z coordinate vertically upwards, the geostrophic balance is expressed as follows (Pickard and Emery, 1990):

$$fv = \frac{1}{\rho} x \frac{\partial p}{\partial x} \qquad (2)$$

$$fu = -\frac{1}{\rho} x \frac{\partial p}{\partial y} \qquad (3)$$

These are the east and north pressure balances respectively. Here p is the ocean pressure, u and v are the horizontal velocities in the x and y directions, ρ is the sea-water density, and f is the local Coriolis parameter defined as

$$f = 2\Omega \sin \Phi \qquad (4)$$

where Ω is the earth rotation rate (7.272×10^{-5} rad s^{-1}) and Φ is the latitude.

Equations (2) and (3) express that water flowing horizontally experiences a horizontal force perpendicular to the direction of flow, tending to move it to the right in the northern hemisphere, and to the left in the southern hemisphere.

For currents at the sea surface, the horizontal pressure gradient is proportional to the ocean topography slope (ζ), and $p = \rho g \zeta$ therefore equations (2) and (3) become:

$$v = \frac{g}{f} x \frac{\partial \zeta}{\partial x} \qquad (5)$$

$$u = -\frac{g}{f} x \frac{\partial \zeta}{\partial y} \quad . \qquad (6)$$

Equations (5) and (6) show how the ocean topography measured from a satellite altimeter can be directly related to geostrophic currents. The ocean topography is related to the sea surface height (SSH) and the geoid through the following relation: ζ = SSH - Geoid. The SLA is equal to the sea surface height less the mean calculated for the period studied. Therefore, the ocean topography is related to the SLA through the following relation: ζ = SLA + Mean – Geoid. If we assumed that the mean and the geoid are similar, we can calculated the geostrophic currents using the SLA data set.

The magnitude of the absolute geostrophic current is calculated using:

$$| v | = \frac{g}{f} \sqrt{\left(\frac{\partial SLA}{\partial y} \right)^2 + \left(\frac{\partial SLA}{\partial x} \right)^2} \quad . \qquad (7)$$

Equation (7) was used to calculate the magnitude of the absolute geostrophic velocity using the sea level anomaly derived from the satellite altimetry. A center finite difference method was used to estimate the derivatives from the grided SLA values.

E. METHODOLOGY

The Sea Level Anomaly data set distributed by AVISO was used for the period beginning on October 3, 1993 (cycle 2) and ending on October 9, 1996 (cycle 149) for T/P; and for the period beginning on October 8,1992 (cycle 6) and ending on December 23, 1993 (cycle 18) for ERS-1 (phase C). Another data set used was for the period beginning on April 28, 1995 (cycle 2) and ending on June 20, 1996 (cycle 13) for ERS-1 (phase G). Data were selected for the area between latitudes 9° and 22° N and longitudes 60° and 90° W (see Figs. 7 and 8). These data were corrected by AVISO, and a summary of the corrections applied is shown in Table 2. These corrections were discussed in section B, and more information can be found in Fu et al. (1994) and AVISO (1997).

CORRECTIONS	METHOD USED FOR CORRECTION (T/P)	METHOD USED FOR CORRECTION (ERS-1)
Orbit	NASA Joint Gravity Model (JMG) 3	D-PAF precise orbit with reference to TOPEX ellipsoid
Dry troposphere and Inv. Barometer effect	From ECMWF	From ECMWF (upgrade; "old" products used FNMO)
Wet troposphere	From TMR radiometer	From ATSR-M radiometer
Ionosphere	From dual-frequency altimeter for TOPEX ; and from DORIS for POSEIDON	BENT model
Sea State Bias	BM4 formula (Gaspar et al., 1994)	Phase C: 5.5% of SWH Phase G: BM3 formula
Ocean tide and loading tide	CSR 3.0 (empirical model derived by the University of Texas)	CSR3.0 model (update)
Solid Earth Tide	Cartwright and Tayler model (1971)	Cartwright and Tayler model (1971)

Table 2. Correction applied by AVISO to the T/P and ERS-1 data set (after AVISO, 1997)

AVISO also applied the along-track repeat analysis to calculate the sea level anomalies. This demonstrated one of the main objectives of the AVISO, that is to provide users with data corrected for all geophysical, media and instrument effects as well as for orbit errors.

Using the software provided by AVISO, the T/P and ERS-1 data for the Caribbean area were extracted. Since the altimeter height measurement fails over land, the island and landmass were flagged. All flagged data were eliminated in order to reduce the probability of data error. After that, the data were interpolated to a fixed geographical grid (0.5° latitude x 0.5° longitude) using an inverse distance square weighting technique. A radius of 2 miles for the T/P data set and a radius of 1 mile for the ERS-1 data set were selected. These values were selected as the best parameters after trying many combinations of grid size and radius. The inverse distance square weighting technique gave a data set that we can easily contour, and allowed us to create maps of sea surface height anomalies for each cycle (10 days period for T/P and 35 days period for ERS-1). We used the middle day of each cycle to identify the date of the cycle.

Once all the information was obtained, the spatially averaged SLA of each cycle was calculated and plotted with respect to time. A seasonal cycle was observed due to steric effects (Fig. 11) related to the dilatation and contraction of the surface layer due to heat fluxes. High values were observed during summer and low values during winter. Seasonal cycles in sea level were expected because the primary driving forces of the ocean currents, winds and heating, have strong seasonal cycles. In order to better describe the mesoscale circulation features, an annual harmonic function was estimated by fitting,

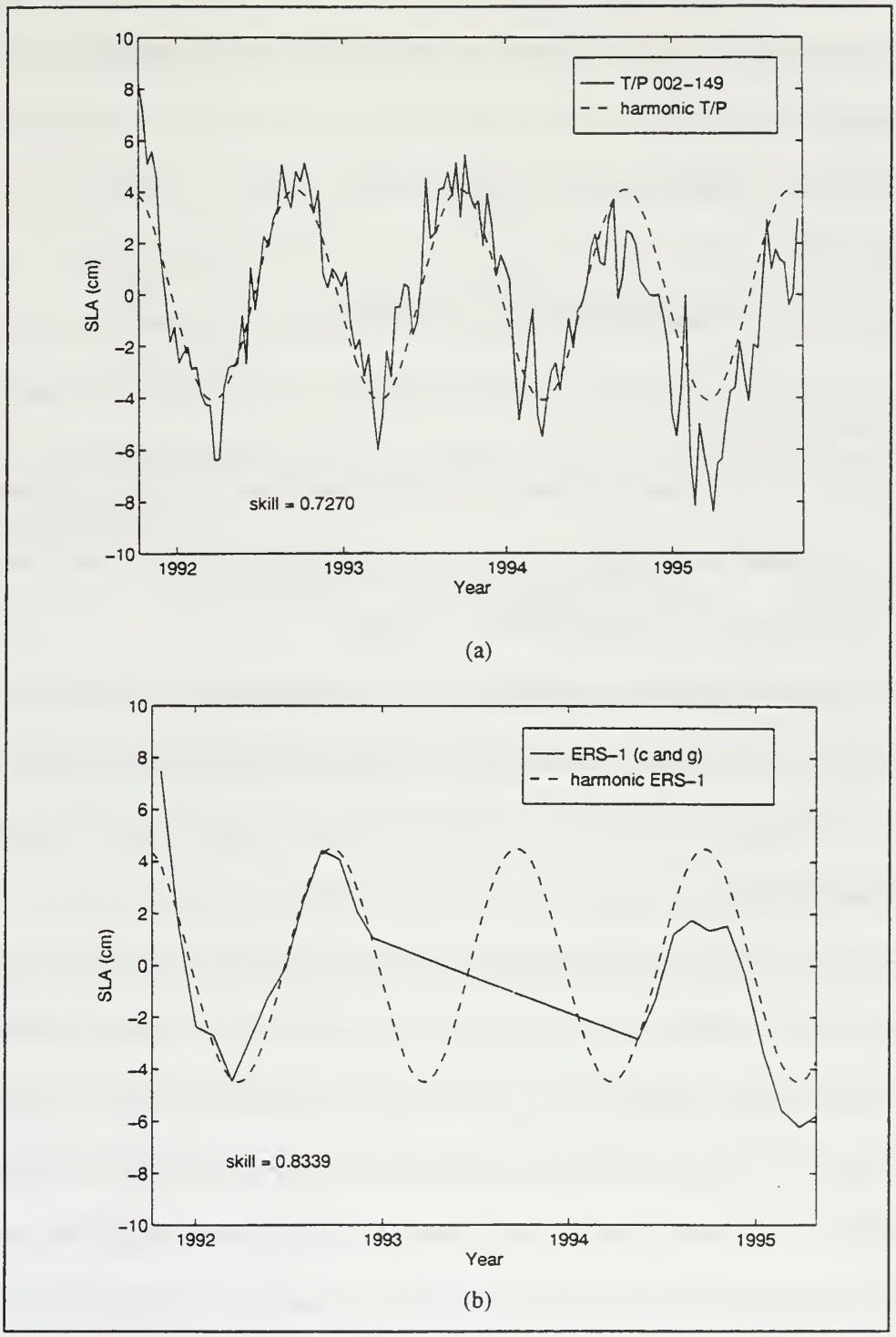

Figure 11. Spatially averaged SLA for each cycle and annual harmonic function computed for T/P (a) and ERS-1 (b). The straight line indicates no data during this period.

in the least square sense, a seasonal cycle to the mean SLA from each cycle (Fig. 11). The harmonic function, *y(t),* corresponding to the best fit is as follows for T/P and ERS-1, respectively:

$$y(t) = 4.0963 * \cos\left(\frac{2\pi t}{365} + 1.7494\right) \qquad (8)$$

$$y(t) = 4.5006 * \cos\left(\frac{2\pi t}{365} + 1.6965\right) \quad , \qquad (9)$$

where t is the time in days.

The value of this harmonic function was calculated for each cycle and subtracted from the interpolated data. Maps of sea surface height anomalies were then created for each 10 day (T/P data) and 35 day (ERS-1 data) cycles.

The ratio of the variance explained by this seasonal harmonic function over the total variance of the data, that is the skill, is 0.7270 for T/P and is 0.8339 for ERS-1. The skill value oscillates between 0 and 1. Values close to unity means a better fit of the data to the harmonic function.

A Sea Surface Temperature (SST) data set provided by JPL was used to compare the surface thermal features to the SLA fields. This data set was collected during the World Ocean Circulation Experiment (WOCE) and contains SST averaged over five days and 0.5 degrees in latitude and longitude, over the global ocean. The area between 9° – 22° N and 60° – 90° W was extracted. Unfortunately, the location of the grid points was at 0.25 and 0.75 of latitude and longitude; in contrast to the location of the grid points in the SLA grid that was at 0.0 and 0.5 of latitude and longitude. The data were derived from the 5-channel Advanced Very High Resolution Radiometer (AVHRR) instrument on

board the polar orbiting satellites NOAA-7, NOAA-9, NOAA-11 and NOAA-14, using the 'NOAA/NASA Pathfinder SST' algorithm, version 4.0 for 1990-1995, and version 4.1 for 1996 (Zlotnicki and Case, 1998). SST images were plotted on the same days as the SLA. A spatially averaged SST for each cycle was calculated and plotted against time. A seasonal cycle was observed in the mean SST values. SST and SLA maps were compared and correlation coefficients between both parameters were computed. An annual harmonic function was estimating by fitting, in the least square sense, a seasonal cycle to the spatially averaged SST values. The harmonic function, *y(t)*, corresponding to the best fit for SST is:

$$y(t) = 27.6189 + 1.0480 * \cos\left(\frac{2\pi t}{365} + 1.9816\right) \qquad (10)$$

The SLA seasonal cycle was delayed by 13 days with respect to the SST seasonal cycle. This delay was calculated using the difference in phase between the harmonic functions.

Temporal contours of SLA, at fixed latitude, longitude or specific satellite pass, were created. These plots help to track the mesoscale features, confirm their position and estimate their velocities and movement. Also, the standard deviation at each geographical data point for the SLA grid was calculated for the period studied and discussed.

Finally, SLA anomalies were compared to data from two drifters released in the southeastern Caribbean Sea between March and October 1996. These drifters were WOCE-TOGA systems dropped to a nominal depth of 15 m (Poulain et al., 1996). The data were generously provided by Dr. Olson of the University of Miami. Ten-day trajectory segments for each drifter were superimposed on the contemporaneous SLA

maps. These trajectories were compared with the sense of circulation derived from SLA maps. Geostrophic velocities computed using the SLA information were compared with the drifter velocities.

IV. RESULTS AND DISCUSSIONS

We now compare T/P data with ERS-1 and SST data to justify the use of T/P images to track the mesoscale features. Then, we select sequences of cycles to follow mesoscale features and describe quantitatively and qualitatively the mesoscale features detected in the Caribbean area. Finally, we calculate the geostrophic velocities from the sea surface height anomalies and compare the magnitude and direction of the geostrophic velocity with 10-day drifter trajectory segments for the same period.

A. COMPARISON ERS-1 AND T/P

Before we discuss the contour sequences to follow mesoscale features over time, it is important to remember that the variability must be added to the mean sea level. Between the northern and the southern part of the Caribbean Sea there is a difference in dynamic height of about 20 dynamic centimeters (Wust, 1963; Gordon, 1967). As a result, the positive and negative values do not reflect actual dynamic height. Instead the positive and negative values reflect height over a reference level, which is the mean sea surface height computed previously to derive the SLA.

A comparison between T/P and ERS-1 was done. For a single satellite mission, temporal resolution and spatial resolution are opposing each other. The higher the temporal resolution, the lower the spatial resolution, and vice versa. As shown in Figs. 7 and 8, the ERS-1 data have a smaller ground track separation than the T/P data; however, the spatial resolution is high but the temporal resolution is small (repeat cycles are separated 35 days). On the other hand, the T/P data have a repeat cycle of orbit of almost 10 days. In the first contour sequence (Figs. 12, 13 and 14), maps from T/P data were

compared to maps from the ERS-1 data and almost the same features were observed. As a result, it was decided to only use the T/P data set hereafter because it provides a better temporal resolution in order to follow the mesoscale features. Also the T/P data were continuous during all the period studied while the ERS-1 data were interrupted for more than one year.

B. COMPARISON T/P AND SST

The average SST in the Caribbean Sea is around 27.5° C with a variation around +/- 1° C. One must remember that infrared SST measures the skin temperature of the ocean surface (less than 5 mm deep). Mesoscale features may only be detected for a limited period of time in infrared images because heat loss to the atmosphere makes them difficult to identify. Also the SST data set was an average of information collected from 4 different satellites over a period of 5 days; therefore, some of the features have been smoothed out by this process. Some features were identified in the SST images but it was not possible to track the movement of features in the Caribbean Sea using SST. The more important characteristics observed in the SST images were: (1) Upwelling along the Venezuelan coast between January and April of each year (dry season) which agree with Gordon (1967) and Leaman (1998); (2) High temperatures (around 30° C) south of Cuba and near the Yucatan Strait mainly between June and October. These characteristics are shown in Fig. 15. Also it was observed that the Golfo de los Mosquitos was often covered by clouds. In this region heavy rainfall is expected.

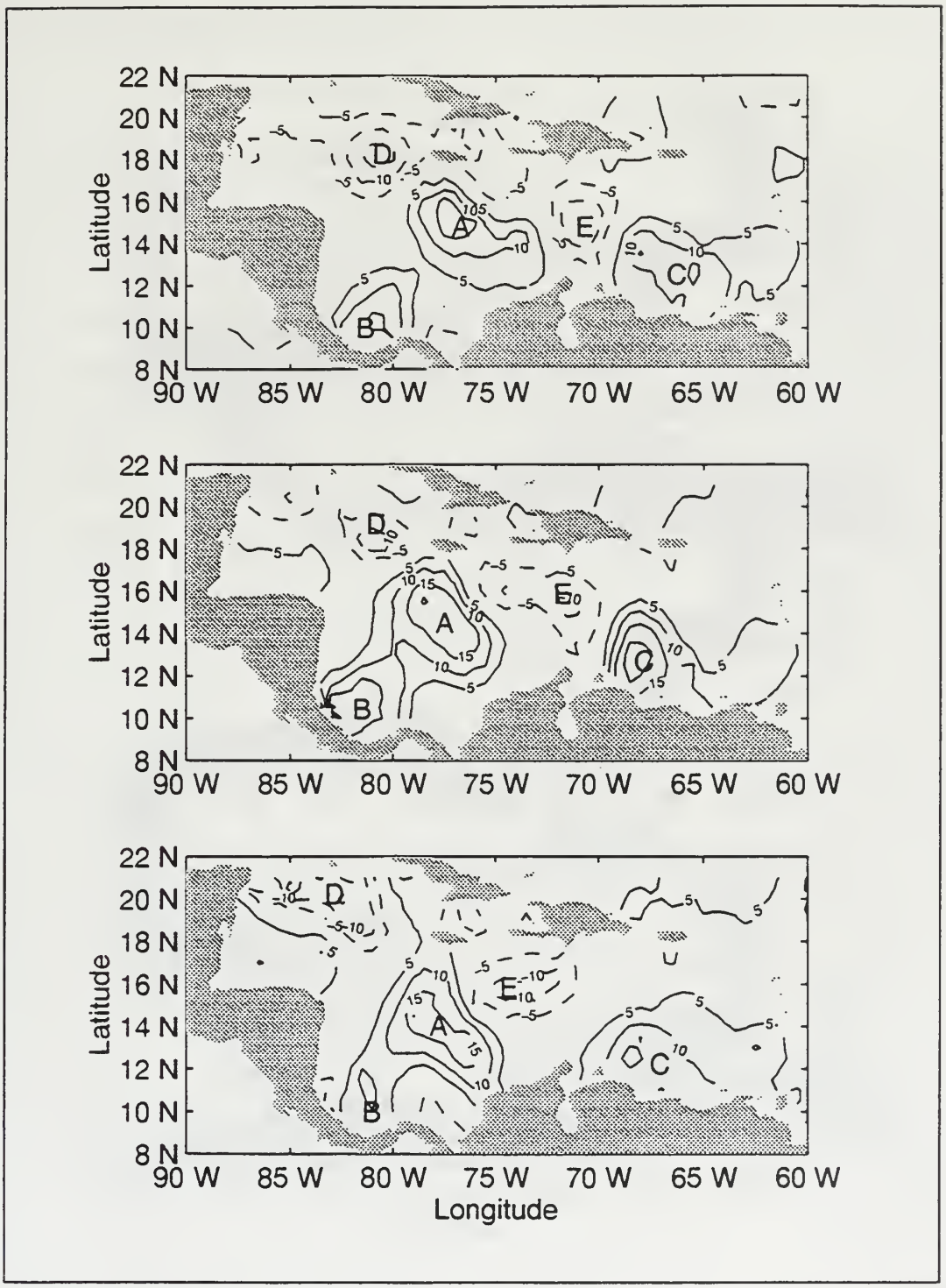

Figure 12. Sea Level Anomaly (T/P) contour map sequence from October 26 to November 16, 1992. Contour interval is 5 cm.

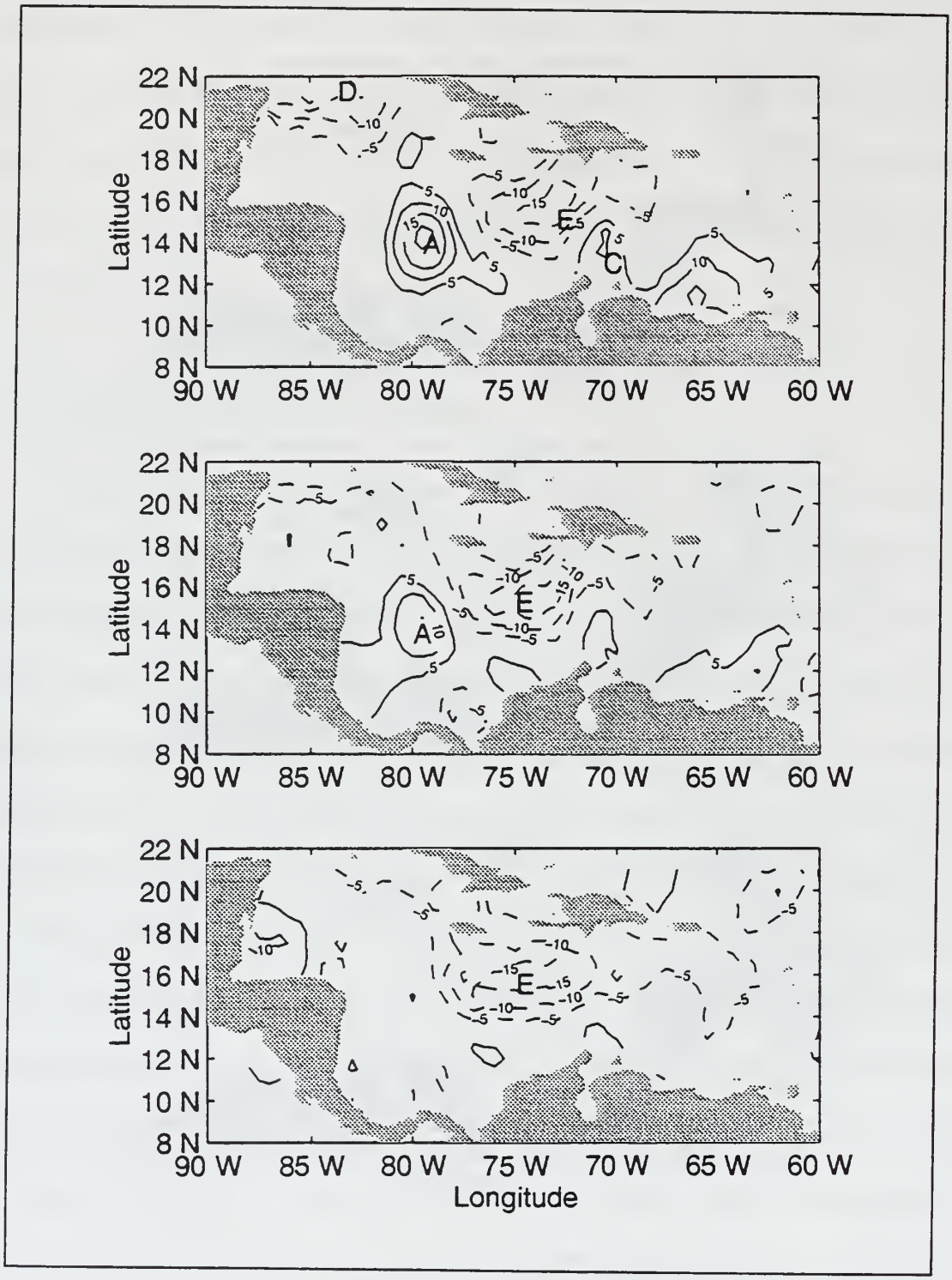

Figure 13. Sea Level Anomaly (T/P) contour map sequence from November 26 to December 16, 1992. Contour interval is 5 cm.

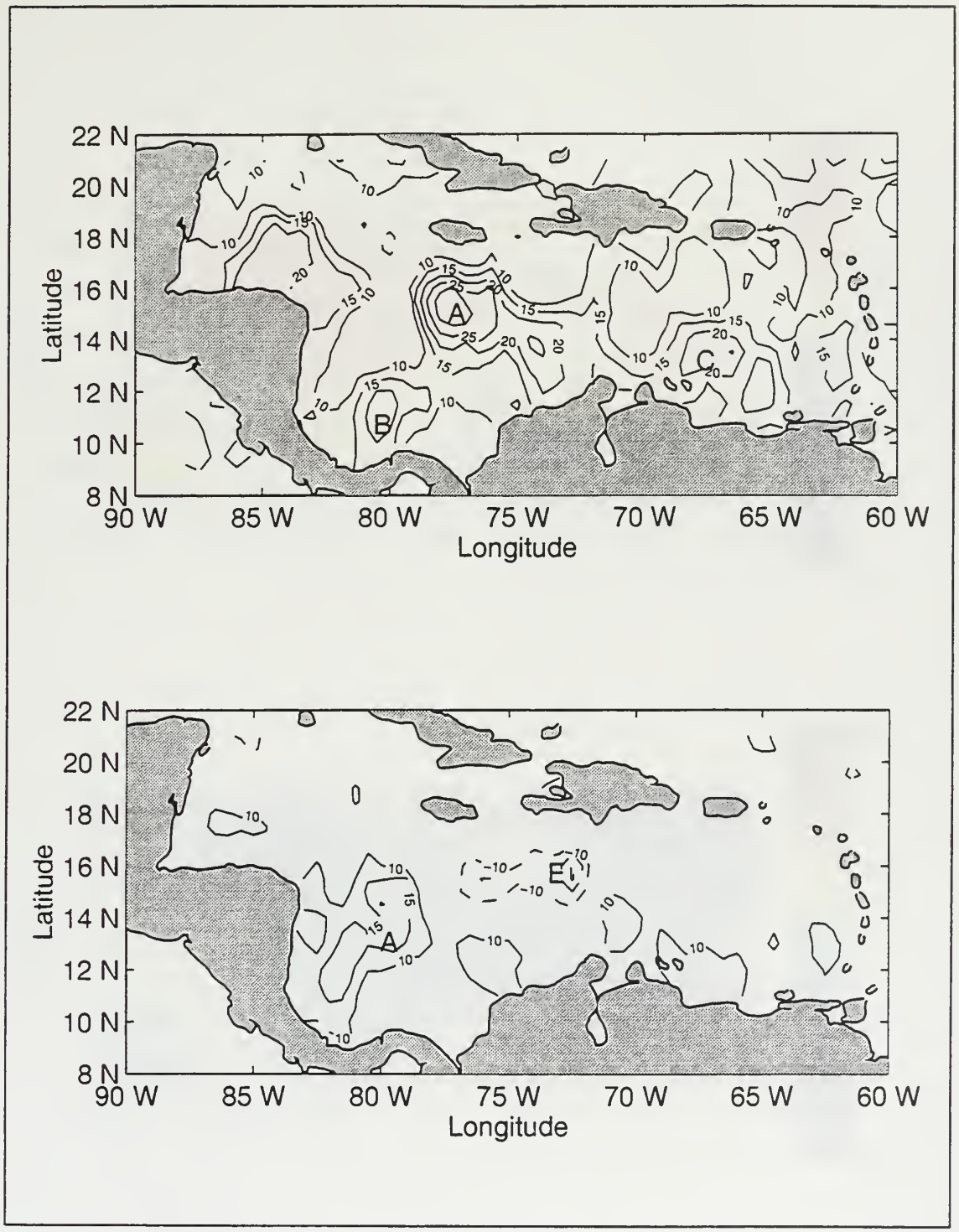

Figure 14. Sea Level Anomaly (ERS-1) contour map sequence from October 25 and November 28, 1992. Contour interval is 5 cm.

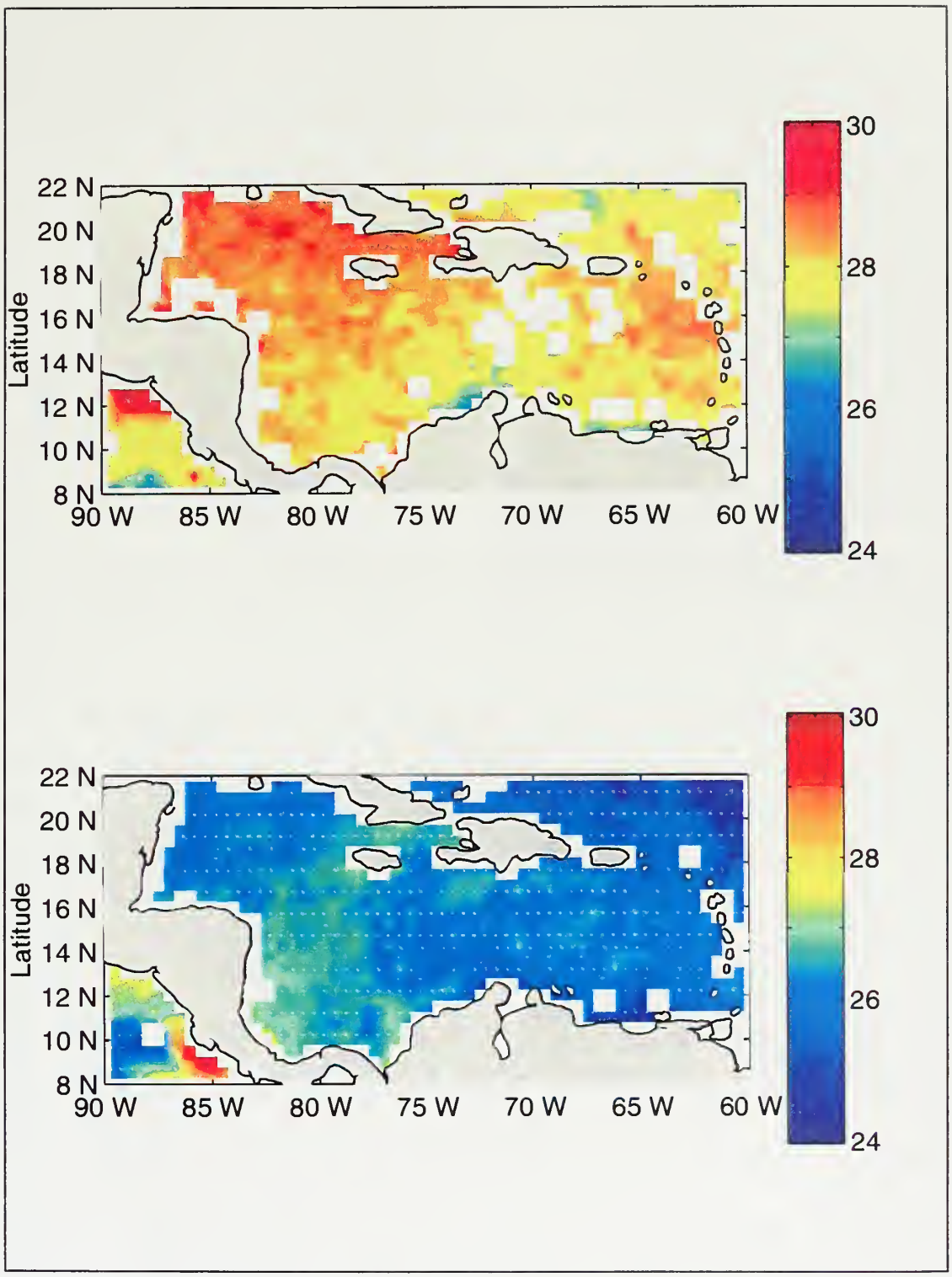

Figure 15. SST Images for the Caribbean Sea. Top image corresponds to November 6, 1992 and bottom image corresponds to February 15, 1993

The correlation coefficients between SLA and SST were computed at the closest geographical location before and after removing the seasonal cycle for both data sets. The correlation coefficient contour maps are shown in Fig. 16.

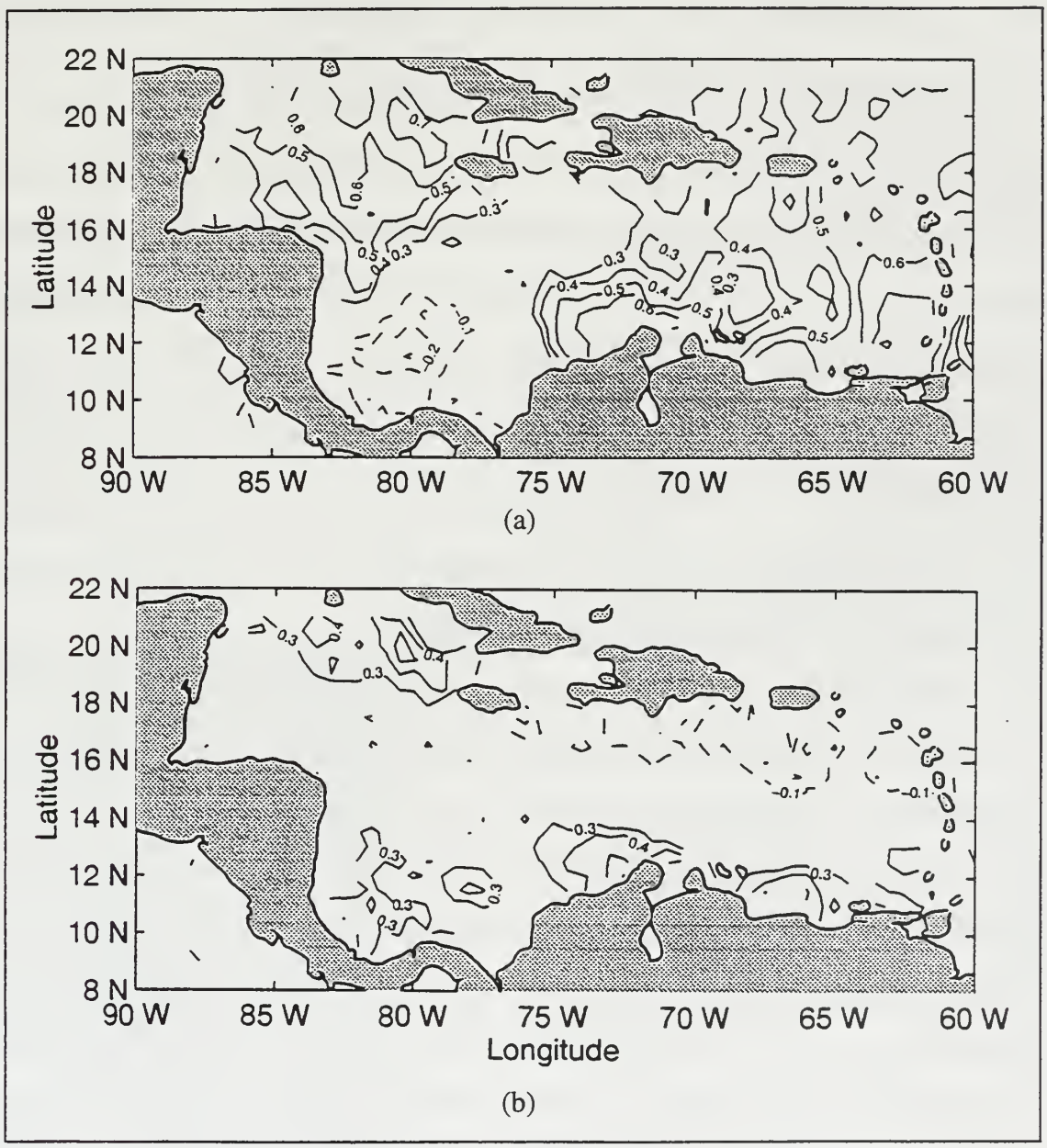

Figure 16. Maps of correlation coefficient between SLA and SST without removing (a) and with removing (b) the seasonal cycle in each data set. Contour interval is 0.1.

Correlation coefficients were higher before removing the seasonal cycle because SST also has a seasonal cycle. Maximum values (> 0.5) were found along the coast of Venezuela, near Yucatan Strait and in the southeastern Caribbean Sea.

C. QUALITATIVE DESCRIPTION OF MESOSCALE FEATURES

A summary of all features detected in the Caribbean Sea is shown in Table 3. The initial location (Lat. / Long.), initial sea surface height anomaly (in cm), size (in km), duration (in days and cycles) and main characteristic of all features detected are included. Also a movie with all cycles used in this work was created. The most representative features were selected based on strength, periodicity and location. Three contour sequences were selected to describe the main characteristics of the mesoscale variability in the Caribbean Sea. These maps were produced after the seasonal cycle was removed.

Date 1st appear	Cycle	Initial SLA (cm)	Initial location (Lat. / Long.)	Size (km)	Duration (days / cycles)	Comments
7-Oct-92	2	15	15° N / 76° W	130	60 / 7	Move West, keep intensity 15, increase 20 before die, size ~150 km
7-Oct-92	2	10	10° N / 80° W	200	40 / 5	Increase to 15 and keep value. Stationary in Golfo de los Mosquitos
17-Oct-92	3	10	12° N / 65° W	30	40 / 5	Max value = 20, Move west along Venezuelan coast
27-Oct-92	4	-10	15° N / 71° W	40	110/12	Move West, Int. increase to -15 and keep this value for 40 days
27-Oct-92	4	-15	18° N / 81° W	30	30 / 4	Move NW towards Yucatan St., int decrease -10, size ~50 km
26-Dec-92	10	-10	20° N / 82° W	20	50 / 6	Move NW, go up -15 for 10 days and then continue moving at -10
25-Jan-93	13	15	10° N / 81° W	20	30 / 4	Stationary in Golfo de los Mosquitos, Increase to 20, size ~210 km
3-Feb-93	14	10	17° N / 75° W	45	10d / 2	Move West. Increase to 15 and disappear
3-Feb-93	14	10	13° N / 68° W	60	20 / 3	Move West, keep intensity of 10 during short life
13-Feb-93	15	-10	14° N / 62° W	50	100 / 11	Appear at East part, move to NW towards Pto. Rico, Max value -15
23-Feb-93	16	10	13° N / 77° W	20	20 / 3	Move West. Increase to 15 and disappear, size ~40 km

Date 1st appear	Cycle	Initial SLA (cm)	Initial location (Lat. / Long.)	Size (km)	Duration (days / cycles)	Comments
15-Mar-93	18	10	14° N / 72° W	90	80 / 9	Move West, increase to 15 and keep value for 40 days, size ~60 km
12-Jun-93	27	10	15° N / 71° W	50	90 / 10	Move West, increase intensity to 15 for 20 days, size ~90 km
12-Jun-93	27	10	16° N/66.5°W	65	50 / 6	Move West, keep intensity of 10 during life, size ~80 km
12-Jul-93	30	-10	15° N / 76° W	25	30 / 4	Move NW, keep intensity of –10, travel 300 km, size 50 km
21-Aug-93	34	-10	14° N / 73° W	45	80 / 9	Move West, after 30 days intensity grows to –20 for 40 days
31-Aug-93	35	-10	10° N / 81° W	110	30 / 4	Stationary, Golfo de los Mosquitos, Int. grows to –15 until disappear
31-Aug-93	35	10	19° N / 83° W	30	40 / 5	Move West, form at North near Yucatan Strait
20-Sep-93	37	10	18° N / 80° W	30	20 / 3	Move W,NW, keep value of 10
20-Sep-93	38	-15	14° N / 68° W	30	20 / 3	Move West, keep value of -15 during short life
30-Sep-93	38	10	16° N / 75° W	50	10d / 2	Short life, seems that doesn't move
29-Oct-93	41	20	17° N / 69° W	15	10d / 2	Keep same location south of Hispanola Island
18-Nov-93	43	-15	15° N / 74° W	50	60 / 7	Strong until cycle 46, Move West, keep value of -15 and slow decay
6-Jan-94	48	10	16.5° N/74°W	25	50 / 6	Move West, Intensity constant and small size (30 km)
6-Jan-94	48	-10	13° N / 71° W	35	10d / 2	Move North, suddenly disappear
4-Feb-94	51	15	12° N / 80° W	80	30 / 4	Stationary, Strong until cycle 53
14-Feb-94	52	-10	14° N / 73° W	70	70 / 8	Move West, value of -10 during his life
6-Mar-94	54	-10	18° N / 84° W	35	20 / 3	Move NW towards Yucatan St. Grows to -20 near Yucatan St.
5-Apr-94	57	10	14° N / 73° W	25	50 / 6	Move West, increase Intensity to 15 for 30 days, suddenly disappear
15-Apr-94	58	10	10° N / 81° W	45	20 / 3	Stationary, seems to join eddy BB after 20 days
5-May-94	60	-10	18° N / 83° W	10	20 / 3	Move West, small size (~30 km) and intensity (-10)
23-Jun-94	65	-15	13° N / 78° W	25	100 / 11	First move SW then became stationary at same location than others
3-Jul-94	66	-10	15° N / 74° W	60	50 / 6	Move West, keep size (~50 km), intensity increase to -15
3-Jul-94	66	15	16° N / 78° W	60	20 / 3	Move North, from initial location towards Jamaica.
3-Jul-94	66	15	19° N / 81° W	25	30 / 4	Move NW, go up to 20 until disappear

Date 1st appear	Cycle	Initial SLA (cm)	Initial location (Lat. / Long.)	Size (km)	Duration (days / cycles)	Comments
13-Jul-94	67	15	15° N / 60° W	70	50 / 6	Appear at East part, move to W,NW towards south Puerto Rico
23-Jul-94	68	10	16° N / 73° W	35	70 / 8	Move West, Intensity increase to 15 for 40 days, Small size (~15Km)
23-Jul-94	68	10	14° N / 68° W	30	160 / 7	Long life. Move West, intensity increase up to 20. Travel farther.
23-Jul-94	68	-15	12.5° N/71°W	50	120 / 13	Start at Venezuela coast, move NW and then West. Int -15, max -25
20-Sep-94	74	-10	13° N / 68° W	50	130 / 14	Move NW, very similar to II. Intensity –10 and size 40 km.
20-Oct-94	77	10	10° N / 78° W	60	60 / 7	Stationary. Start at east of usual location, then move. Max int 15
16-Jan-95	86	-10	15° N / 74° W	40	20 / 3	Move West, keep same value of -10, small size
5-Feb-95	88	10	12° N / 80° W	40	20 / 3	Grow to 25 after 10 days. Stationary (Golfo de los Mosquitos)
5-Feb-95	88	10	17° N / 72° W	70	150 / 16	Move W at N (up 16°), then go NW towards Yucatan St, size:80-90
24-Jun-95	102	15	14° N / 65° W	50	90 / 10	Move West at S (down 13°) Move about 10°(~1000 km), size 120 km
24-Jul-95	105	-10	14° N / 78° W	140	40 / 5	Move West, keep same intensity of -10 during its life
23-Aug-95	108	-10	16° N / 74° W	70	60 / 7	Move West at N, keep value of -15, travel around 500 km, size 130km
1-Sep-95	109	-20	14° N / 68° W	25	30 / 4	Move West, intensity decrease to -15, and stay there, size 30 km
31-Oct-95	115	10	13° N / 76° W	120	20 / 3	Move West, short life
10-Dec-95	119	-10	16° N / 77° W	100	50 / 6	Move NW towards Yucatan St, grow to –15, size 90-120 km
6-Apr-96	131	10	14° N / 74° W	50	40 / 5	Move West, intensity -10, size 110 km, travel ~300 km
16-Apr-96	132	-10	14° N / 74° W	80	30 / 4	Move West, small size (~30 km) and intensity (-10)
4-Jun-96	137	-10	10° N / 81° W	50	60 / 7	Stationary, Grow up to -15
24-Jun-96	139	-10	14° N / 74° W	70	80 / 9	Move West, Seems to join eddy YY, grow up to -20 to -25 before die
4-Jul-96	140	10	15° N / 65° W	50	60 / 7	Move West, then to SW, die in Venezuela coast, Grow up to 15
14-Jul-96	141	-10	15.5° N/70°W	60	20 / 3	Move to SW, short life
24-Jul-96	142	15	16° N / 75° W	35	20 / 3	Move West, keep size (~40 km) but reduce intensity to 10
23-Aug-96	145	-10	15° N / 74° W	30	40 / 5	Move West, strong intensity of -20 for 30 days, present until cycle 149

Table 3. Main characteristics of SLA features detected in the Caribbean Sea

The first sequence is from October 27 (cycle 04) to December 16 (cycle 09), 1992 (Figs. 12 and 13). On October 27, five anomalies were detected of which three were positive anomalies (anticyclonic, clockwise) marked as A, B and C; and two were negative anomalies (cyclonic, counterclockwise) marked as D and E. During the duration of the sequence, features A, C and D moved to the west at average speeds of 14 cm/s. Feature A disappeared after 40 days and feature C disappeared after 30 days. Feature E was present during the entire sequence and kept moving to the west until February 13, 1993, which was almost four months before it disappeared.

Feature D moved to the northwest toward the Yucatan Strait at speed close to 20 cm/s. Intensification in strength and speed were observed as the eddy approached the Yucatan Strait. It seemed to continue toward the Gulf of Mexico. Feature B appears to be a stationary anticyclonic eddy in the Golfo de los Mosquitos as suggested by Kinder (1985). Nyusten and Andrade (1993) described a cyclonic quasi-permanent feature in this area. However, our data suggest that anticyclonic and cyclonic features alternate their passage in the central part of the Caribbean Sea.

The same period of time is presented in Fig. 14 but using the ERS-1 data. All features described before for the first sequence were found in the sequence using ERS-1 data. The location, size and intensity of many of the features are similar but it is very difficult to follow the movement of these features using images more than one month apart. For this reason, the T/P data were preferred to follow the mesoscale features in the Caribbean Sea.

The next sequence is from August 12 (cycle 70) to September 30 (cycle 75), 1994 (Figs. 17 and 18). On August 12, six anomalies were detected of which three were positive (anticyclonic) identified as F, G and H; and three were negative (cyclonic) identified as I, J and K. Features F, G, H, J and K moved to the west at average speeds around 14 cm/s. The alternate pattern between cyclonic and anticyclonic features in the central part of the Caribbean Sea was again observed. Feature J disappear after 10 days near the coast of Nicaragua as suggested by Carton and Chao (1998). Feature H disappeared after 20 days. Feature K grew in amplitude up to –25 cm. During this sequence, the quasi-permanent feature in the Golfo de los Mosquitos was again observed (feature I) but this time showing counterclockwise rotation (cyclonic).

The last sequence considered is between July 14 (cycle 141) and September 01 (cycle 146), 1996 (Figs. 19 and 20). On July 14, four anomalies were observed of which three were negative (cyclonic) identified as L, M and N; and one was positive (anticyclonic) identified as O.

Feature L is the quasi-stationary eddy of the Golfo de los Mosquitos showing counterclockwise rotation (cyclonic). Features M, N and O moved to the west at average speeds of 12 cm/s. Following feature N, it was detected that it seemed to disappear on August 13 and reappear on August 23. This discontinuity in the eddy trajectory could be caused by the failure of the T/P data to capture small eddies or rings located between the satellite tracks. On July 24, an anticyclonic feature identified as P was detected to the south of Cuba. It also propagated to the west with apparent speed of 15 cm/s.

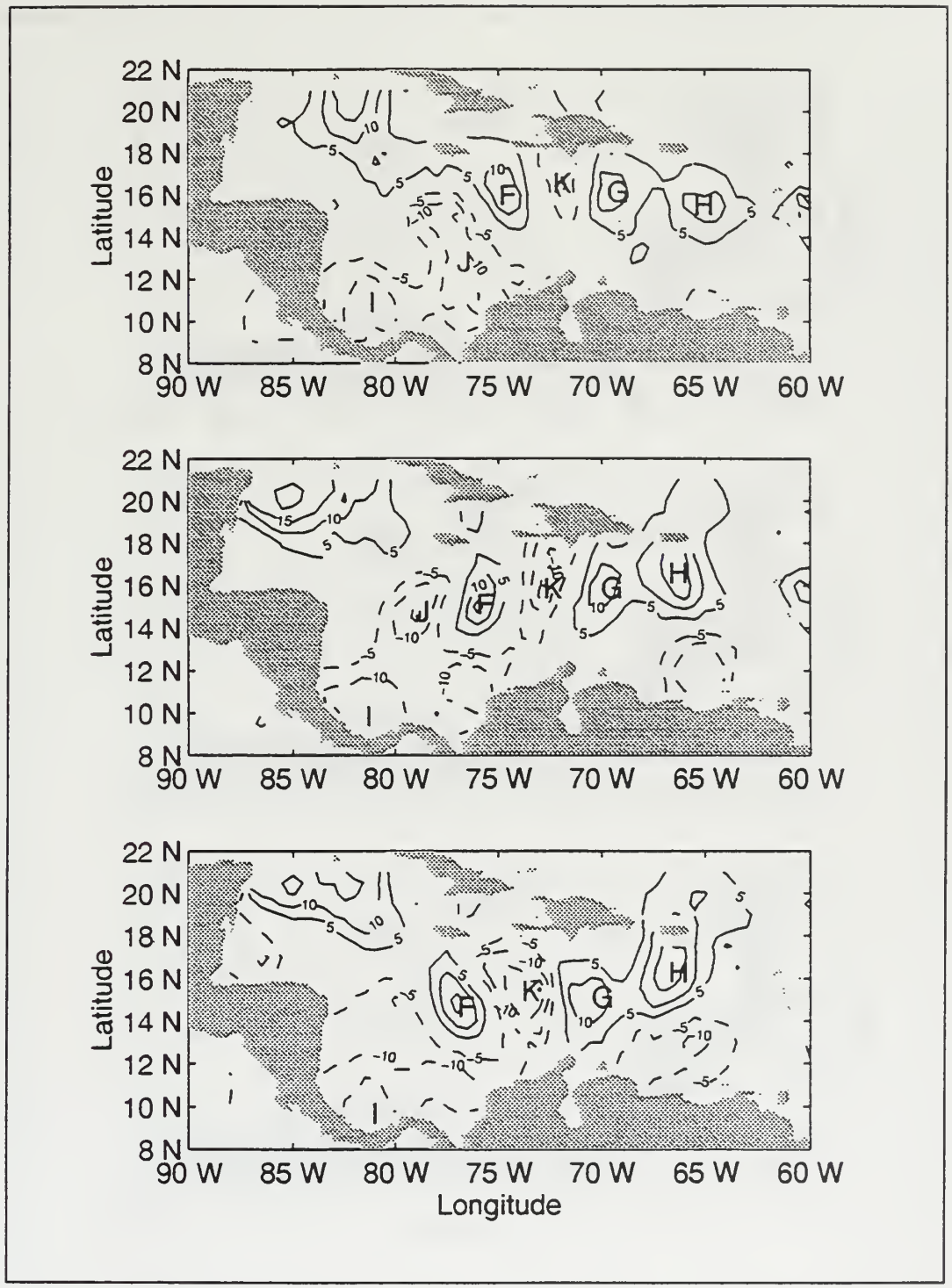

Figure 17. Sea Level Anomaly (T/P) contour map sequence from August 12 to September 01, 1994. Contour interval is 5 cm.

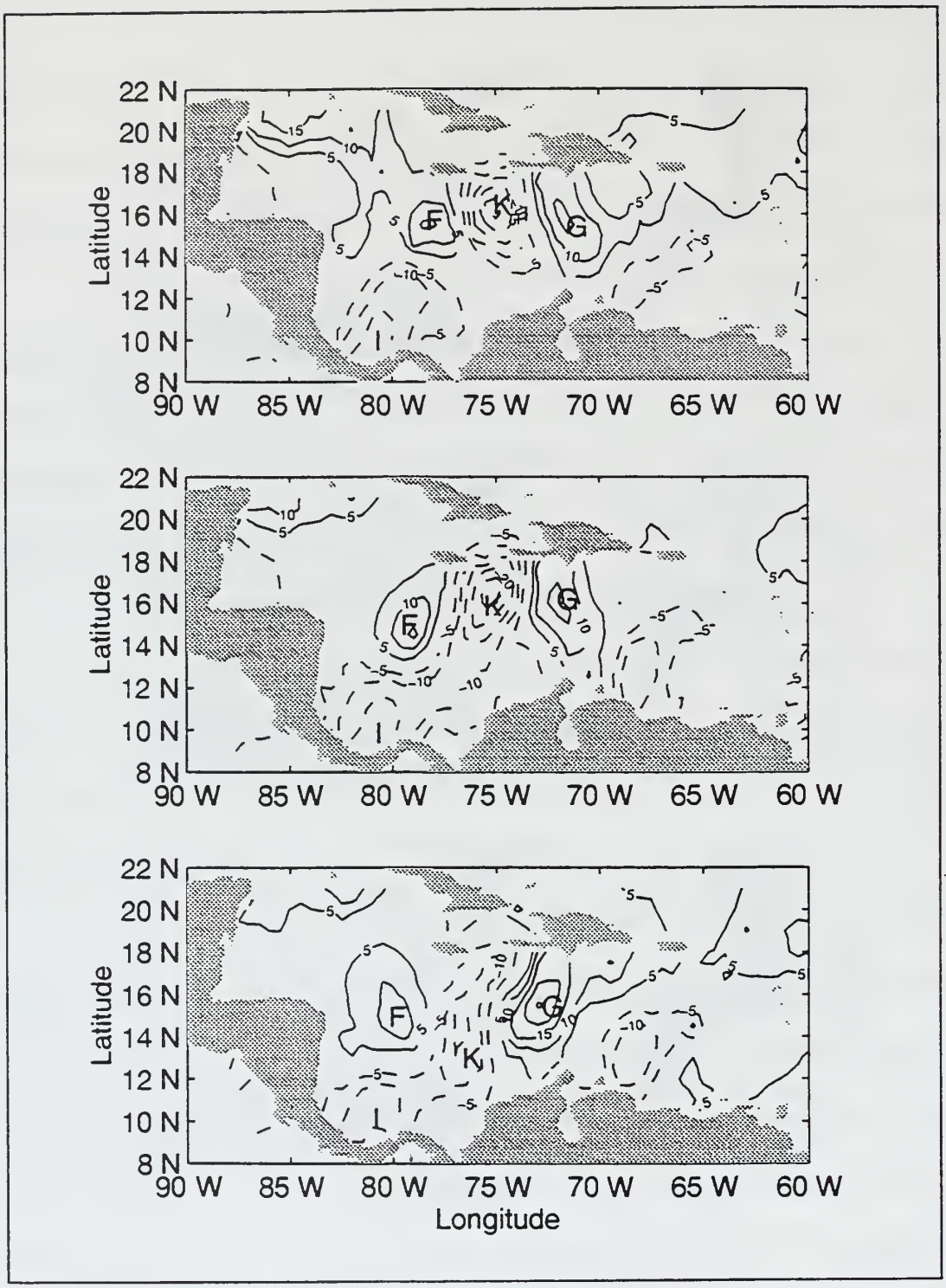

Figure 18. Sea Level Anomaly (T/P) contour map sequence from September 10 to September 30, 1992. Contour interval is 5 cm.

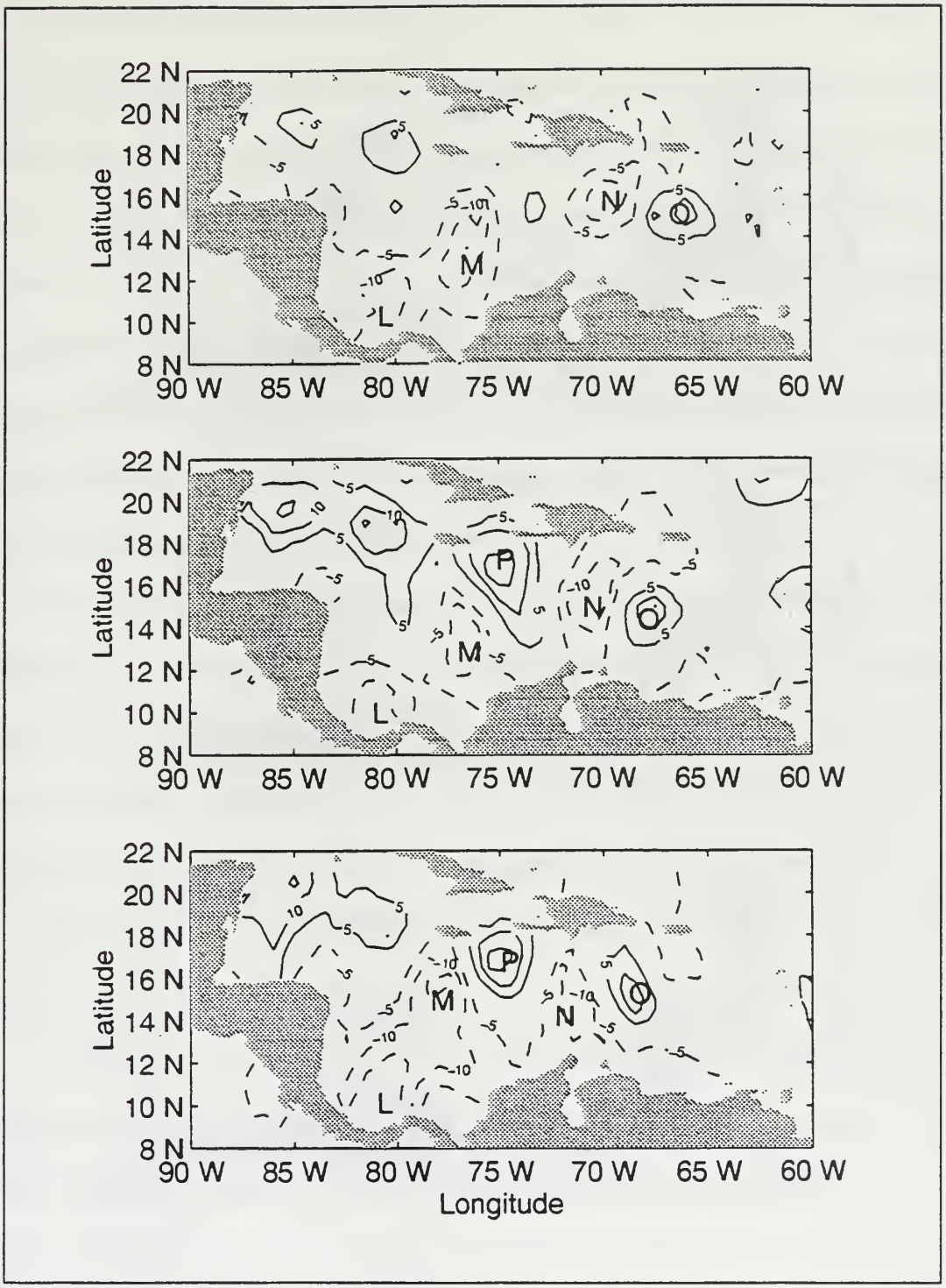

Figure 19. Sea Level Anomaly (T/P) contour map sequence from July 14 to August 03, 1996. Contour interval is 5 cm.

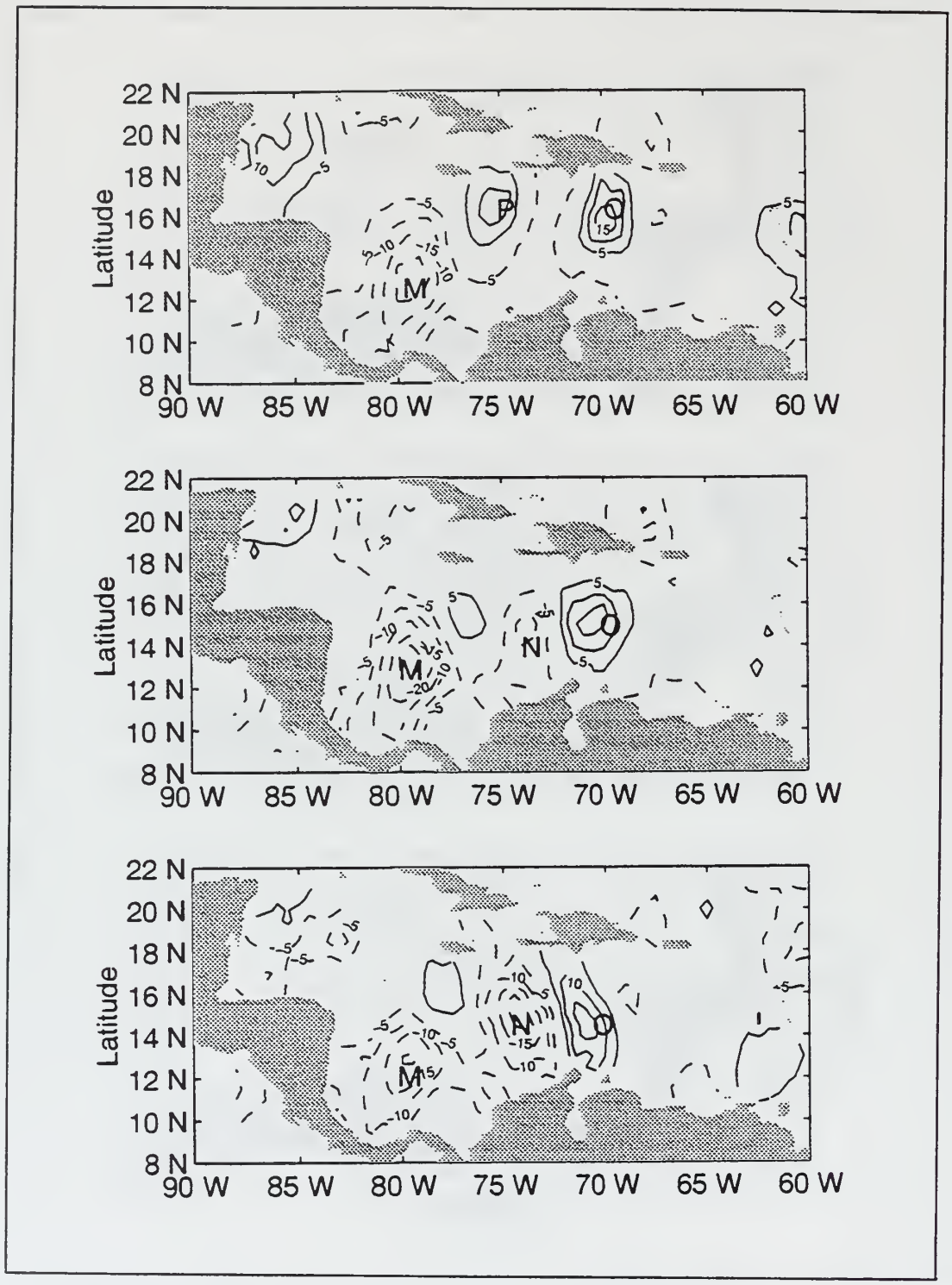

Figure 20. Sea Level Anomaly (T/P) contour map sequence from August 13 to September 01, 1996. Contour interval is 5 cm.

D. QUANTITATIVE DESCRIPTION OF MESOSCALE FEATURES

In order to determine the movement of the features in the central part of the Caribbean Sea, a SLA contour plot with respect to time and longitude at a fixed latitude 15.5° N was examined. Figure 21 suggests that features move to the west with speeds between 10 and 15 cm/s. Speeds were calculated by using the approximate slope of the lines that indicate the westward movement of the features detected. These values were lower that the values found by Molinari (1981) and Kinder (1983) in the same region using satellite-tracked drifters (~ 50 cm/s), but they agree well with the average speed of 15 cm/s found by Nystuen and Andrade (1993).

The alternation of cyclonic and anticyclonic features is also seen in Fig. 21. This alternation pattern is seen all year but during the months of July and January (rainy season) it seems to be stronger. Some of the mesoscale features observed in Fig. 21 traveled completely across the Caribbean (63° - 82° W) in about six months. In Fig. 21, it is also observed that some of the mesoscale features originated near the eastern part of the Caribbean Sea (between 63° and 65° W) but the height magnitude of these eddies is generally small (between 10 and –10 cm).

Relatively strong meanders and eddies were found in the central part of the Caribbean. Molinari et al. (1981) also found eddies propagating in the same area, but they reported that eddies appear to form near the large topographic features such as the Beata and Aves Ridge (Figs. 1 and 2) that separates the Venezuelan and Colombia basins. Perhaps the Aves Ridge contributes to eddy generation in the eastern Caribbean. The

most likely mechanism for generation of the eddies is the seasonal change in the wind field induced by ITCZ meridional escursions.

In order to examine the behavior of the features in the Golfo de los Mosquitos, space-time diagrams of the sea level anomaly for passes 141 and 204 (tracks A and B in Fig. 9) were examined. Figure 22 suggests that this is a quasi-permanent feature, which appears at various times throughout the period studied between 10° and 13° N under these particular passes. This feature is detected only because it moves; otherwise it would be removed by the geoid removal technique that removes truly permanent features. This eddy was reported at the same position by Wust (1963), Molinari et al., (1981), Kinder (1983) and Nyustean and Andrade (1993) but the sense of rotation reported by these authors was different. Wust and Kinder found a counterclockwise rotation, while Molinari and Nyustean and Andrade found a clockwise rotation. Kinder believed that an eddy was always present in this area and it could be cyclonic or anticyclonic.

As seen in Fig. 22, the sense of rotation of this feature varies with the seasons. During the dry season (November-April), anticyclonic features are more likely and during the rainy season (June-October) cyclonic features are predominant. This change may be related to the seasonal movement of the ITCZ and the consequent change of where the trade winds are found in the Caribbean Sea. As a result, the trade winds may cause a large gyre in the Golfo de los Mosquitos labeled by Leaman (1998) as the Panama-Colombia Gyre (PCG). Leaman stated that the PCG may exhibit major changes over the seasons and may sometimes reverse direction. New information will be gathered

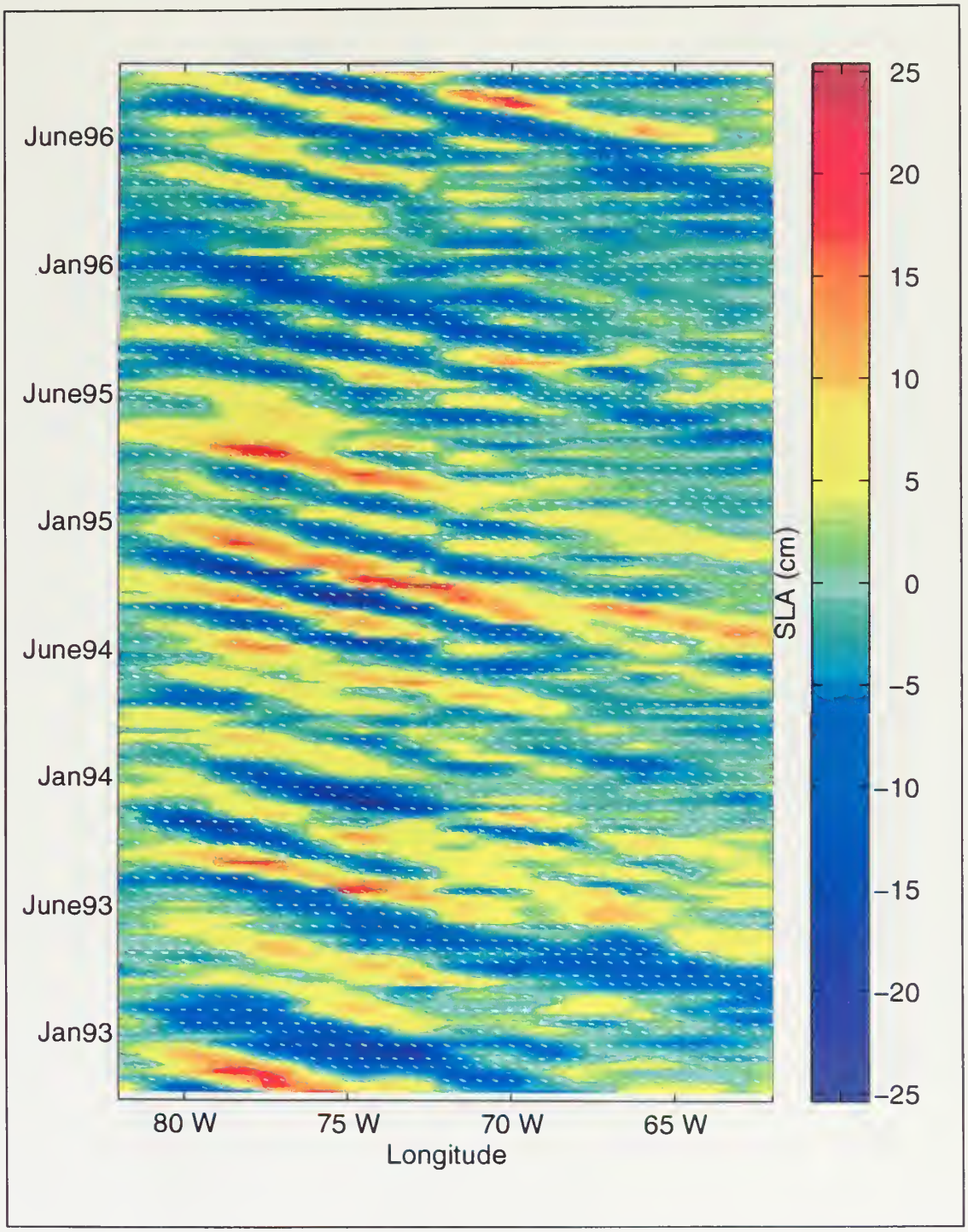

Figure 21. SLA contour plot with respect to time and longitude at a fixed latitude 15.5° N. The westward movement of the cyclonic (blue) and anticyclonic (red) features is observed.

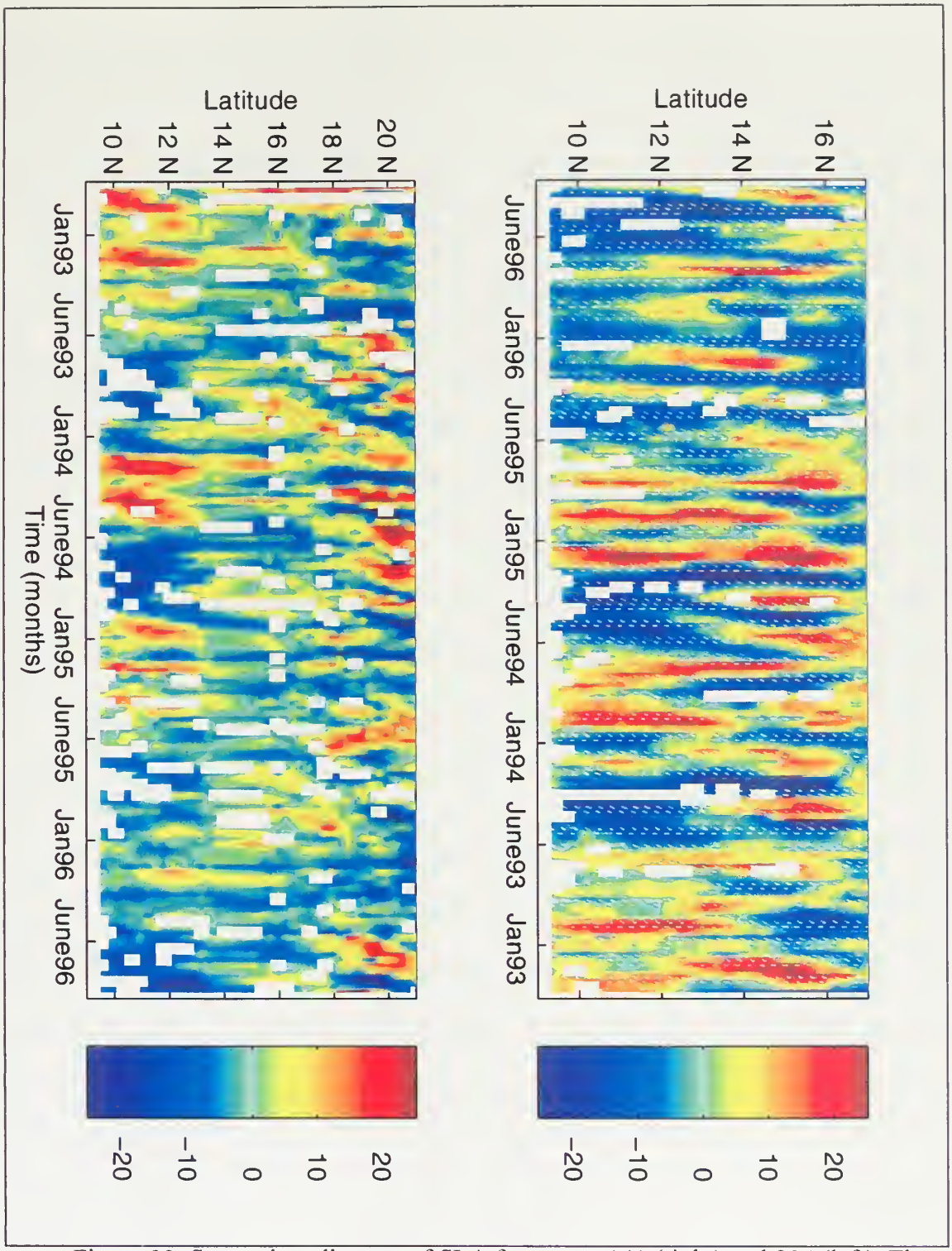

Figure 22. Space-time diagram of SLA for passes 141 (right) and 204 (left). The stationary eddy is located between 10° and 13° N.

using drifters that will be launched in the southwestern Caribbean Sea as an initial effort to describe the PCG and its changes. Drifters used in the past did not sample this area very well and a separate set of drifters will be launched in the southwestern Caribbean Sea to obtain a more uniform coverage of the region.

Another way to quantify the SLA variability is to plot its standard deviation as a function of geographical location. The SLA standard deviation was calculated for each grided point along the entire Caribbean and contoured as shown in Fig. 23. Maximum values were found south of Hispanola and Jamaica islands in the Colombia basin where the meandering and eddy activity were more intense. Most of the eddies detected in this work showed an intensification as they go through this area. In addition, maximum values were found in the southwestern Caribbean Sea where the quasi-permanent eddy was detected. Large variability was found in the Central Caribbean Sea where many eddies were detected.

Minimum values were found in the eastern Caribbean Sea where eddy activity was expected but not observed. A reason for the lack of observed eddy activity in this area could be that the features may be newly created in this area and consequently they are smaller than the resolution of T/P. Also minimum values were found along the coast of Nicaragua where Carton and Chao (1998) suggested that many eddies dissipate as they pass over the Nicaraguan Rise.

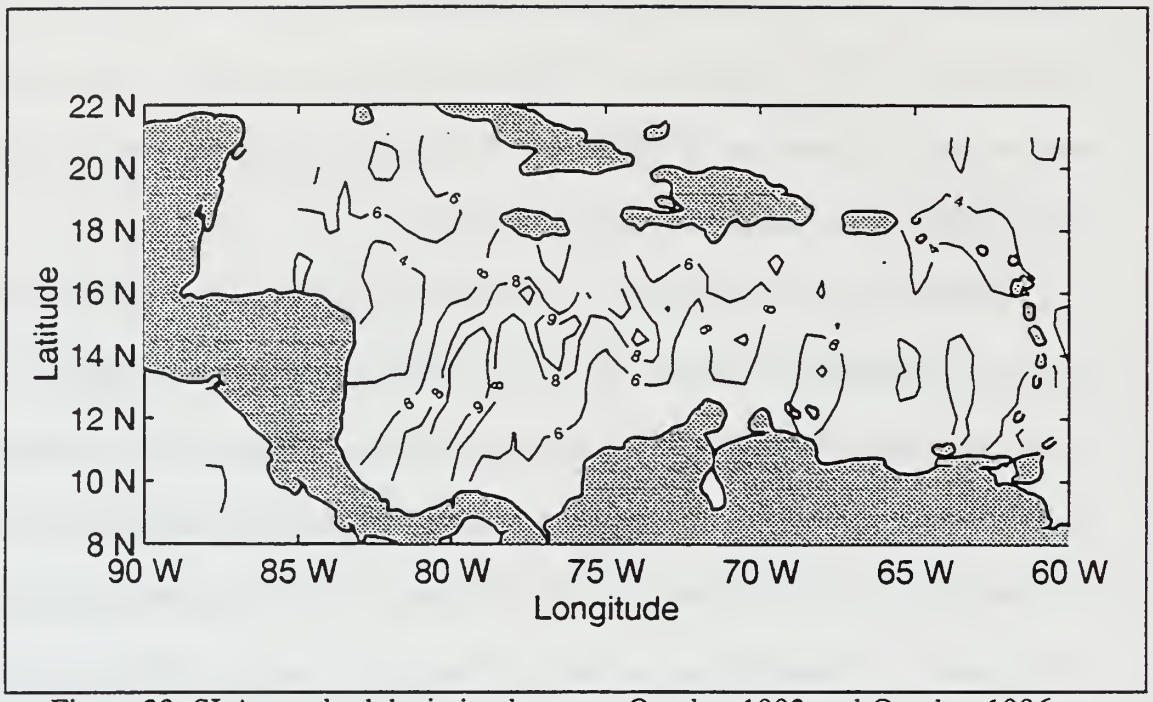

Figure 23. SLA standard deviation between October 1992 and October 1996.

E. COMPARISON OF T/P WITH DRIFTERS

Finally, the information provided by two drifters released in the southeastern Caribbean Sea between March 96 and October 96 was compared to the SLA contour maps for the same period. The entire drifter tracks over the Caribbean Sea are shown in Fig. 24. Both drifters traveled westward from their released location near the Lesser Antilles and they showed a tendency to meander or loop in a similar way to previous satellite-tracked drifters shown in Figs. 3 and 4.

Neither of the two drifters reached the southwestern Caribbean Sea, and they were carried through the Caribbean Sea and Yucatan Strait by the Caribbean Current. The

velocities of the drifters were between 25 and 60 cm/s, and they agree with the averages found by Molinari (1981) and Kinder (1983). The drifter tracks show different scales of spatial variability. It was found that drifter tracks and SLA from T/P agree very well in some areas and disagree in others.

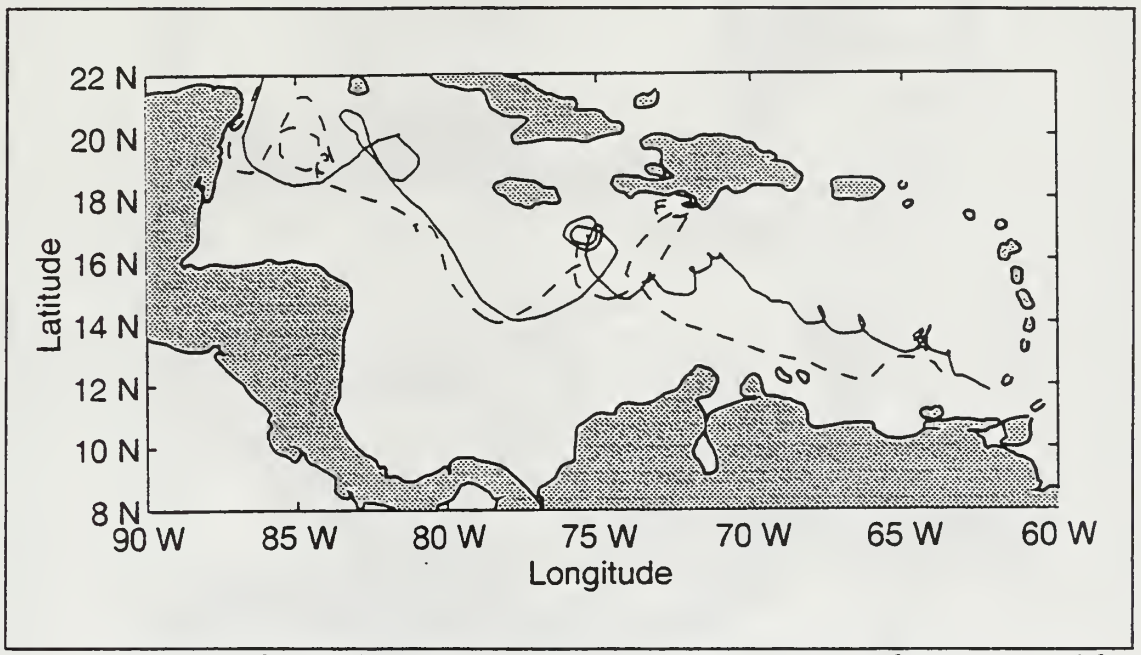

Figure 24. Drifter tracks in the Caribbean Sea between March96 and October96

A good agreement is shown in Fig. 25 in which 10-day drifter trajectory segments are superimposed on contemporaneous SLA maps. In the sequence beginning July 24, the trajectory described by one of the drifters showed a clockwise rotation around a anticyclonic feature defined by the SLA maps. During the time period of the sequence (about a month) the drifter got trapped in the center of the anticyclonic feature and turned twice around it before exiting. These two different ways of measuring ocean currents, in-situ measurements (drifters) and remotely sensing measurements (satellite altimetry) presented a good agreement in their information and can be easily combined.

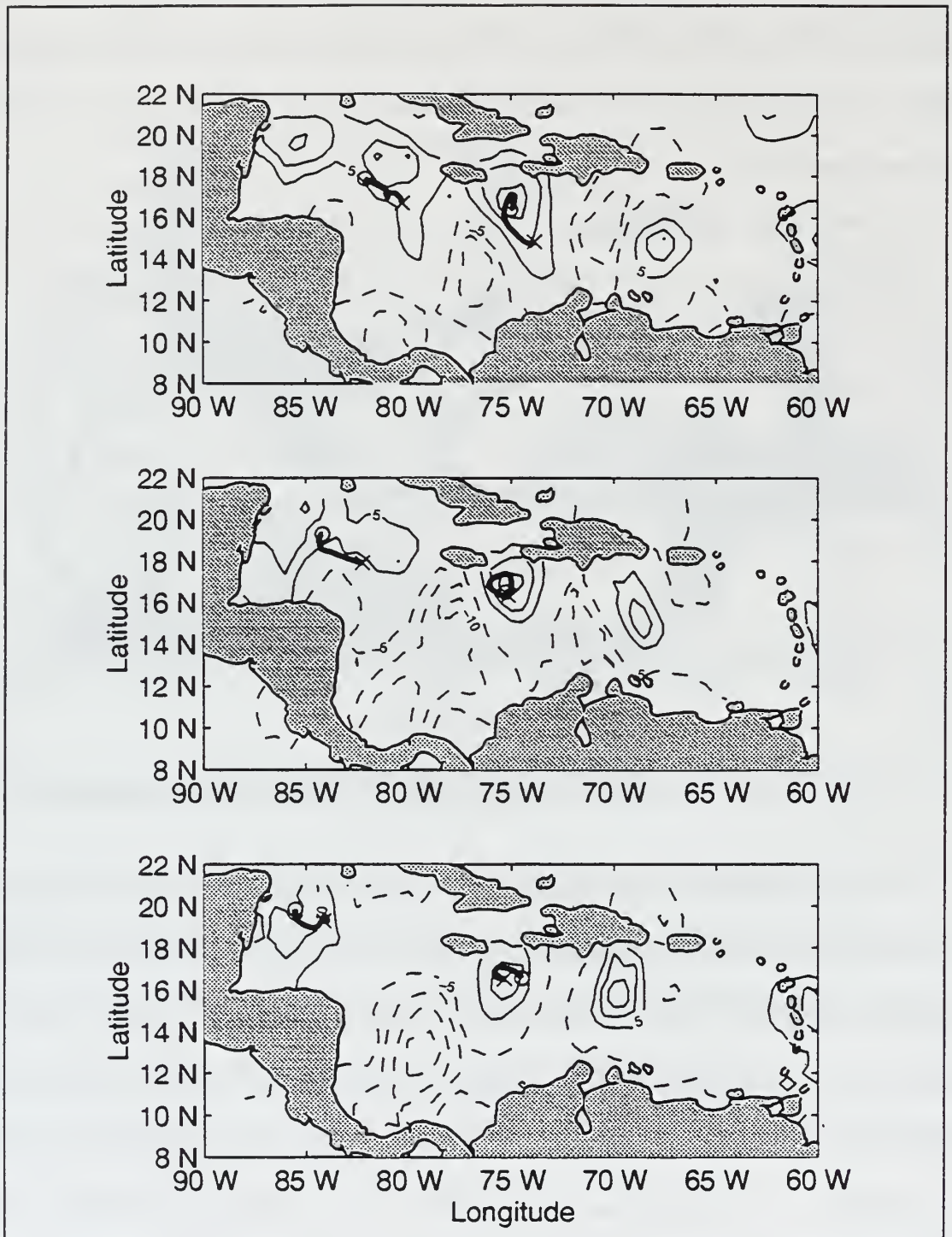

Figure 25. Sequence of 10-day drifter trajectory segments and SLA contour maps from July 24 to August 13, 1996. First and last drifter location are indicated by X and O symbols, respectively.

In contrast, a disagreement between drifter trajectory and satellite altimetry is shown in Fig. 26. One of the drifter trajectories showed propagation to the northwest while the SLA contour map showed small positive and negative values along the drifter trajectory.

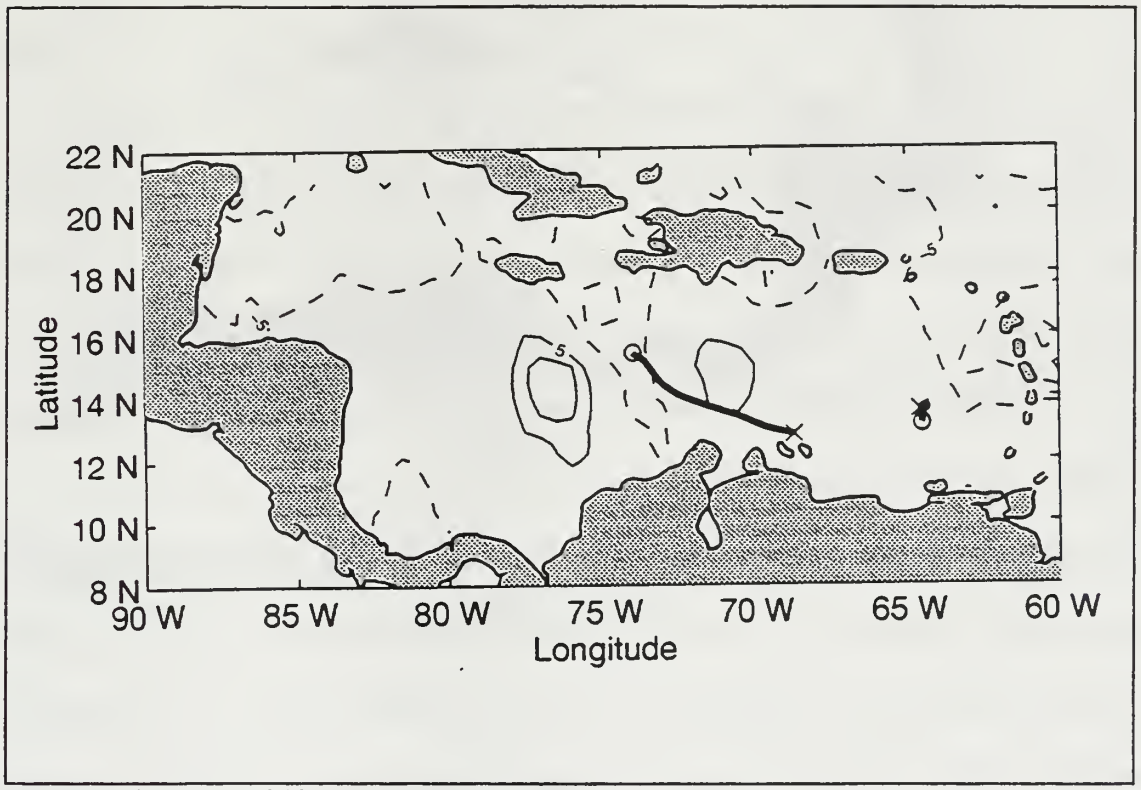

Figure 26. 10-day drifter trajectory segment superimposed over SLA contour map for April 06, 1996. This is an example of disagreement between drifter and satellite altimetry data.

The magnitude of the geostrophic currents derived from SLA was calculated for each cycle using equation (7) and then compared with the average speeds derived from the drifters. Figure 27 shows a contour map of the geostrophic velocity for August 03, 1996 derived from the SLA data. It was found that the magnitude of the geostrophic currents was smaller than the drifter speed by a factor of two. The major reason for the discrepancy between the drifter and satellite altimetry inferred currents is that SLA does

not represent the permanent geostrophic currents and the wind-driven circulation that affect the drifter paths.

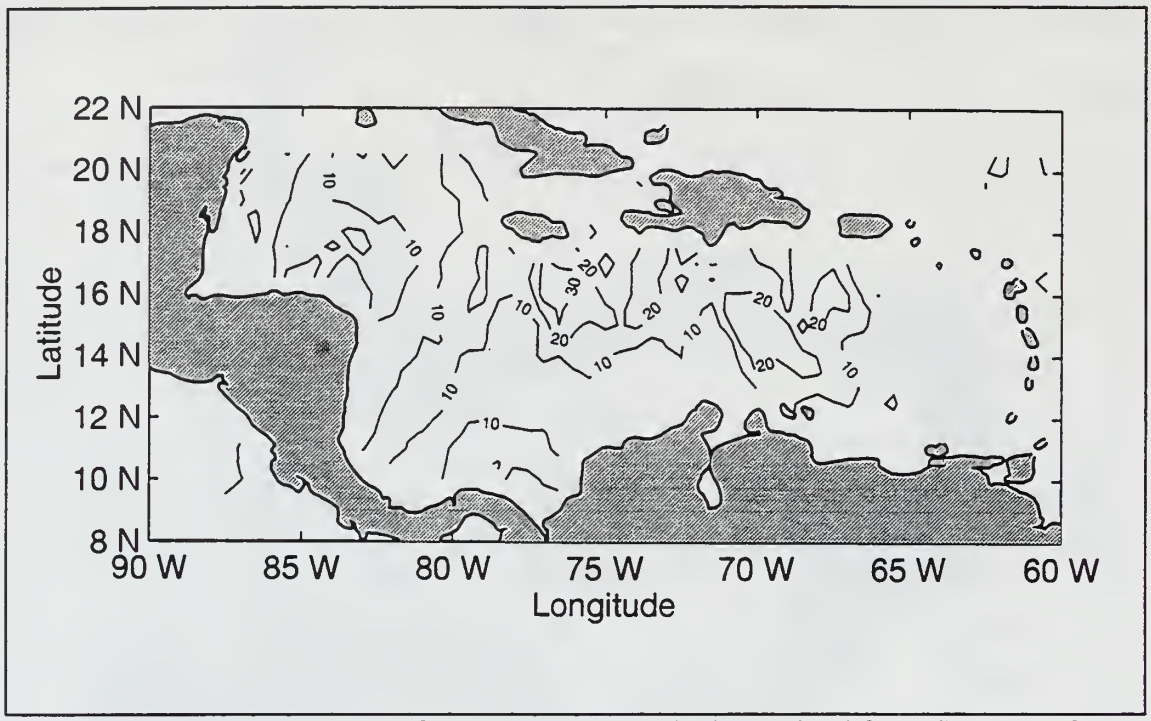

Figure 27. Contour map of the geostrophic velocity derived from SLA data for August 03, 1996.

V. CONCLUSIONS

We have used altimetry data from T/P (October 92 – October 96) and ERS-1 (October 92 – December 93 and April 94 – March 96) to deduce the structure and variability of the mesoscale circulation in the Caribbean Sea. This information was compared with satellite-derived SST and drifter trajectories.

Contour maps of SLA were created for each 10-day cycle for T/P and for each available 35-day cycle for ERS-1. Anticyclonic and cyclonic mesoscale features were detected in the central part of the Caribbean Sea during the entire period studied. These features moved westward at average speeds between 10 and 15 cm/s, growing in amplitude up to 25 cm. Some of the features started near the Beata and Aves Ridges.

A gyre in the Golfo de los Mosquitos was frequently detected at a fixed location. Models have predicted this gyre and it seemed to be a quasi-permanent feature of the western Caribbean associated with the Panama-Colombia Gyre. Because T/P gave only the temporal mesoscale variability of the sea level height in the Caribbean Sea, we derived a modulation in the sense of rotation of this gyre and its variation with the seasons. In addition to the unknown, constant rotation, a clockwise (anticyclonic) rotation was implied for the gyre during the rainy season (June-October), and a counterclockwise (cyclonic) rotation was implied during the dry or windy season (January-April).

No strong mesoscale anomalies were detected in the eastern part of the Caribbean Sea where they were expected. The failure in detecting strong mesoscale activity in this area can be due to the fact that these eddies are newly created in this area and are smaller than the resolution of T/P.

Upwelling was observed near the coast of Venezuela during the dry season. A seasonal cycle was found in the SLA derived from T/P and ERS-1 data due to steric effects. They were expected because the primary driving forces of the ocean currents, winds and heating, have strong seasonal cycles. The SLA seasonal cycle was delayed 13 days with respect to the SST seasonal cycle.

When comparing SLA from T/P to satellite-derived SST, high correlation coefficients (above 0.5) were found along the coast of Venezuela, near the Yucatan Strait, and in the southeastern Caribbean Sea. At others location, low correlation coefficients were found. One reason for the disagreement between SLA and SST could be that SST can be different from the temperature in the upper water column. As a result, the steric effect on SLA is not correlated to SST.

Drifter trajectories contemporaneous with some of the T/P data delineated the westward movement of the Caribbean Current and showed anticyclonic and cyclonic features in the form of small eddies as they traveled through the central Caribbean Sea. A good agreement between SLA and drifters was found for the sense of rotation in strong eddies. In contrast, drifter speeds were typically twice the value of the absolute geostrophic currents calculated from SLA.

VI. RECOMMENDATIONS

In this chapter, we present our recommendations for similar future work based on satellite altimetry.

First, more comparison studies between satellite altimetry, in-situ measurements (drifters, subsurface floats, moorings, etc) and contemporaneous satellite-derived SST fields are recommended to provide accurate description of circulation in mesoscale features.

Second, the implementation of a geodetic mission to obtain a better geoid suitable for oceanographic applications, and the use of a longer mean (more than three years) to calculate the SLA.

Third, the combination of T/P, ERS and future satellite altimetry missions (i.e., GEOSAT Follow-On (GFO) recently launched by the U.S. Navy) information to obtain high temporal and spatial resolution and a better description of mesoscale features in the ocean. When two or more altimetric missions are flying at the same time, the more precise orbit of one of the missions can be used as a reference to increase the spatial or temporal resolution of the other missions.

LIST OF REFERENCES

Andrade, A. C. A., Mesoscale Variability of the Caribbean Sea from GEOSAT, *M. S. thesis*, 55 pages, Naval Postgraduate School, Monterey, 1991.

Atwood, D. K., P. N. Froelich, M. E. Q. Pilson, M. J. Barcelona, and J. L. Vilen, Deep Silicate Content as Evidence of Renewal Processes in the Venezuela Basin, Caribbean Sea, *Deep Sea Research*, vol. 26a, 1179-1184, 1979.

AVISO, Archiving, Validation, and Interpretation of Satellite Data in Oceanography, User Handbook, Sea Level Anomalies (SLAs), 3rd edition, *Publ.* AVI-NT-011-312-CN, Centre. National. d'Etudes Spatiales, Toulouse, France, 1997.

Brucks, J. T., Currents of the Caribbean and Adjacent Regions as Deduced from Drift-bottle Studies, *Bulletin of Marine Science*, vol. 21, 455-465, 1971.

Carton, J. A., and Y. Chao, Caribbean Sea Eddies Inferred from TOPEX/POSEIDON Altimetry and a 1/6 Atlantic Ocean Model Simulation, *Journal of Geophysical Research,* submitted, 1998.

Cartwright, D. E., and R. J. Taylor, New Computations of the Tide-Generating Potential, *Geophysical J. R.. Astronomic Soc.,* vol. 33, 253-264, 1971,

Duncan, C. P., D. K. Atwood, J. R. Duncan, and P. N. Froelich, Drift Bottle Returns from the Caribbean, *Bulletin of Marine Science*, vol. 27, 580-586, 1977.

Froelich, Jr. P. N., and D. K. Atwood, New Evidence for Sporadic Renewal of Venezuela Basin Water, *Deep Sea Research*, vol. 21, 969-975, 1974.

Fu, L., E. J. Christensen, C. A. Yamarone Jr., M. Lefebvre, Y. Ménard, M. Dorrer, and P. Escudier, TOPEX/POSEIDON Mission Overview, *Journal of Geophysical Research*, vol. 99, 24369-24381, 1994.

Gaspar, P., F. Ogor, P. Le Traon, and O. Zanife, Estimating the Sea State Bias of the TOPEX and POSEIDON Altimeters from Crossover Differences, *Journal of Geophysical Research,* vol. 99, 24981-24994, 1994.

Gordon, A., Circulation of the Caribbean Sea, *Journal of Geophysical Research,* vol. 72, 6207-6233, 1967.

Heburn, G. W., T. H. Kinder, J. H. Allender, and H. E. Hurlburt, A Numerical Model of Eddy Generation in the Southeastern Caribbean Sea, in *The Hydrodynamics of Semi-enclosed Seas*, edited by J. C. J. Nihoul, pages 299-328, Elsevier Science, New York, 1982.

Kinder, T. H., Shallow Currents in the Caribbean Sea and Gulf of Mexico as Observed with Satellite-tracked Drifters, *Bulletin of Marine Science*, vol. 33, no. 2, 239-246, 1983.

Kinder, T. H., G. W. Heburn, and A.W. Green, Some Aspects of the Caribbean Circulation, *Marine Geology*, vol. 68, 25-52, 1985.

Le Traon, P. Y., P. Gaspar, F. Bouyssel, and H. Makhmara, Using Topex / Poseidon Data to Enhance ERS-1 Data, *Journal of Atmospheric and Oceanic Technology,* vol. 12, 161-170, 1995.

Leaman, K., cited 1998: Drifters in the Southwestern Caribbean, [Available on-line from http://www.drifters.doe.gov/currents.html]

Metcalf, W. G., Caribbean-Atlantic Water Exchange through the Anegada-Jungfern Passage, *Journal of Geophysical Research*, vol. 81, 6401-6409, 1976.

Metcalf, W. G., M. C. Stalcup, and D. K. Atwood, Mona Passage Drift Bottle Study, *Bulletin of Marine Science*, vol. 27, 586-591, 1977.

Molinari, R. L., M. Spillane, I. Brooks, D. Atwood, and C. Duckett, Surface Currents in the Caribbean Sea as Deduced from Lagrangian Observations, *Journal of Geophysical Research*, vol. 86, 6537-6542, 1981.

Morrison, J. M., and W. D. Nowlin Jr., General Distribution of Water Masses within the Eastern Caribbean Sea during Winter of 1972 and Fall of 1973, *Journal of Geophysical Research*, vol. 87, 4207-4229, 1982.

Morrison, J. M., and O. P. Smith, Geostrophic Transport Variability along the Aves Ridge in the Eastern Caribbean Sea during 1985-1986, *Journal of Geophysical Research*, vol. 95, 699-710, 1990.

Nystuen, J. A., and C. A. Andrade, Tracking Mesoscale Ocean Features in the Caribbean Sea using GEOSAT Altimetry, *Journal of Geophysical Research*, vol. 98, 8389-8394, 1993.

Petterson, L. H., P. Samuel, and A. Drottning, Radar Altimeter Sensors and Methods, in *Oceanographic Applications of Remote Sensing,* edited by M. Ikeda and F. W. Dobson, pages 427-441, CRC Press, Boca Raton, 1995.

Pickard, G. L., and W. J. Emery, *Descriptive Physical Oceanography: An Introduction*, 5th ed., Butterworth-Heinemann, 320 pages, 1990.

Poulain, P.-M, A. Warn-Varnas, and P. P. Niiler, Near-surface Circulation of the Nordic Seas as Measured by Lagrangian Drifters, *Journal of Geophysical Research*, vol. 101, 18237-18258, 1996.

Robinson, I. S., *Satellite Oceanography: An introduction for Oceanographers and Remote-sensing Scientists,* Ellis Harwood Limited, 455 pages, 1985.

Roemmich, D., Circulation of the Caribbean Sea: A Well-resolved Inverse Problem, *Journal of Geophysical Research*, vol. 86, 7993-8005, 1981.

Semtner, A. J., and R. M. Chervin, Ocean General Circulation from a Global Eddy-Resolving Model, *Journal of Geophysical Research,* vol. 97, 5493-5550, 1992.

Sturges, W., Water Characteristics of the Caribbean Sea, *Journal Marine Research*, vol. 23, 147-162, 1965.

Thompson, J. D., T. L. Townsend, A. Wallcraft, and W. J. Schmitz, Jr., Ocean Prediction and the Atlantic Basin: Scientific Issues and Technical Challenges, *Oceanography*, vol.5, 36-41, 1992.

Tomczak, M., and J. S. Godfrey, *Regional Oceanography: An Introduction*, Pergamon, 422 pages, 1994.

Worthington, L. V., A New Theory of Caribbean Bottom-water Formation, *Deep Sea Research*, vol. 3, 82-87, 1955.

Worthington, L. V., Recent Oceanographic Measurements in the Caribbean Sea, *Deep Sea Research*, vol. 13, 731-739, 1966.

Wust, G., On the Stratification and Circulation of the Cold Water Sphere of the Antillean-Caribbean Sea, *Deep Sea Research,* vol. 10, 165-187, 1963.

Wust, G., *Stratification and Circulation in the Antillean-Caribbean Basins*, Columbia University Press, New York, 201 pages, 1964.

Zlotnicki, V., and K. Case, cited 1998: AVHRR Sea Surface Temperature Grids Description, [Available on-line http:// podaac.jpl.nasa.gov/cdrom/woce/ avhrr/docs/avhrrdoc.htm]

INITIAL DISTRIBUTION LIST

1. Defense Technical Information Center 2
   8725 John J. Kingman Rd., STE 0944
   Ft. Belvoir, VA 22060-6218

2. Dudley Knox Library 2
   Naval Postgraduate School
   411 Dyer Rd.
   Monterey, CA 93943-5101

3. Professor Robert Bourke 1
   Code OC/BF Dept. Oceanography
   Naval Postgraduate School
   833 Dyer Rd. Room 328
   Monterey, CA 93943-5122

4. Professor Pierre Poulain 3
   Code OC/PN Dept. Oceanography
   Naval Postgraduate School
   833 Dyer Rd. Room 328
   Monterey, CA 93943-5122

5. Professor Newell Garfield 1
   Code OC/GF Dept. Oceanography
   Naval Postgraduate School
   833 Dyer Rd. Room 328
   Monterey, CA 93943-5122

6. Professor Robin Tokmakian 1
   Code OC/TK Dept. Oceanography
   Naval Postgraduate School
   833 Dyer Rd. Room 328
   Monterey, CA 93943-5122

7. Jefatura de Educación 1
   Comandancia General de la Armada de Venezuela
   Final Av. Vollmer Ed. CGA
   San Bernardino, Ap. Postal 1011, Caracas
   Venezuela

8. Dirección de Hidrografía y Navegación 1
Apartado Postal 6745
Carmelitas, Caracas, Dtto. Federal
Venezuela

9. TF. Luis Pibernat 2
211 Navajo Dr.
Salinas, CA 93906